OPEN ACCESS Freely available online

Investigating Neural Circuitry Using a Compartment-Level Connectivity Map of the Adult *Drosophila* Brain

Wayne S. Pereanu*, Parvez Ahammad, Arnim Jenett, Eugene W. Myers, James W. Truman

Janelia Farm Research Campus, Howard Hughes Medical Institute, Ashburn, Virginia, United States of America

Abstract

An approach taken in *Drosophila* neurobiology has been to perturb genetically addressable sets of neurons and make inferences about the potential function of the affected neurons based on the observed phenotype. Much of this effort has been focused on grossly recognizable structures, such as the mushroom bodies, central complex substructures, antennal lobe, and recently, the antenno-mechanosensory motor center. However, all of these structures comprise only a quarter of the total neuropile volume of the central brain. The field currently lacks information about brain-wide connectivity that could be used as a guide to facilitate in-depth studies of the remaining volume of the central brain. Here we construct a coarse connectivity map of the adult fly brain using a combination of structural elements and developmental information from the semi-differentiated neurons at the late larval stage. The resolution of our map consists of a description of the interconnections between defined neuropile compartments, providing constraints on how information can flow through the central brain. Analysis of network topology and putative functional roles of compartments allow us to measure several network features and compare these to similarly studied nervous systems, including the macaque cortex and cat cortex. We used this analysis to generate and test a precise hypothesis about sensory modulation of a motor behavior. Our results reveal that the premetamorphic connections of the immature lineages prefigure the final pattern of connectivity of the mature brain. This latter finding suggests that brain connectivity can be studied in a development context, since the immature system is greatly reduced in its branching complexity. It is the hope that incorporation of behavioral results into the common structured framework of a connectivity network will allow novel and synthetic predictions, an approach that is likely to prove valuable for similar efforts in other model organisms.

Citation: Pereanu WS, Ahammad P, Jenett A, Myers EW, Truman JW (2011) Investigating Neural Circuitry Using a Compartment-Level Connectivity Map of the Adult *Drosophila* Brain. PLoS Biol 9(1): e1000583. doi:10.1371/journal.pbio.1000583

Academic Editor: Hugo J. Bellen, Baylor College of Medicine, United States of America

Received May 6, 2010; **Accepted** December 7, 2010; **Published** January 25, 2011

Funding: The work was supported by the Howard Hughes Medical Institute. The funders had no role in study design, data collection and analysis, decision to publish, or preparation of the manuscript.

Competing Interests: The authors have declared that no competing interests exist.

* E-mail: pereanuw@janelia.hhmi.org

Introduction

There is a clear relationship in the human brain between anatomically defined brain volumes (Brodmann's cytotechtonic areas [1]) and functional localization [2,3]. A wide range of studies in vertebrates such as the mouse [4], rat [5], canary [6,7], and human [8] have relied on histologically visible landmarks to provide an anatomically relevant foothold for functional investigation.

The brain of *Drosophila melanogaster* has been anatomically divided by several groups [9–12] on the basis of landmarks such as glial processes, axon bundles, and trachea (the latter being topologically similar to the vasculature present in vertebrate brains) into as many as 41 different neuropile compartments [12] excluding the optic lobes. The functional significance of 7 of the 41 compartments (antenna lobe, mushroom body, ellipsoid body, fan-shaped body, protocerebral bridge, lateral horn, and the antenna mechanosensory-motor center) has been experimentally addressed by single-gene mutants as well as by perturbing subsets of neurons and inferring potential function based on the observed phenotype. For example, there is a large body of work implicating each of the three aforementioned central complex substructures in regulating distinct aspects of visual pattern memory and motor control. Pan et al. [13] used RNA interference of the rutabaga adenylyl cyclase selectively in either the fan-shaped body or ellipsoid body and showed that different features of visual pattern memory were processed by the F1/F4 fan-shaped neurons and the R2/R4m ellipsoid body neurons. For the protocerebral bridge, Strauss et al. [14] found that flies mutant for the gene *no-bridge*, which develop a protocerebral bridge that does not fuse at the midline, have a reduced average walking speed and display a lack of leg coordination when turning. Similar work exists for the olfactory system [15] and, more recently, the antenna mechanosensory-motor center [16,17]. Findings from these works indicate that each of the seven compartments are involved in discrete functions, suggesting a functional localization within their respective volumes.

The functions of the remaining neuropile compartments (comprising three-quarters of the volume of the central brain) have not been experimentally addressed. There are two hindrances to work in these remaining areas: a lack of specific tools to target these areas and a lack of general knowledge about brain-wide connectivity that could be used to facilitate experimental design and data interpretation. The first one is being addressed through ongoing work to develop tools to manipulate arbitrary sets of neurons [18], which we take advantage of here. The second issue, which is the focus of this study, requires a description of the origins and terminations of the neurite bundles connecting brain regions,

Author Summary

Work in the nervous systems of several model organisms, from C. elegans to macaque, has led to the description of neural connectivity maps. These efforts have ranged in resolution from individual neurons to compartmentalized volumes of neural tissue. Analysis of the structural constraints present in these maps can reveal mechanisms of how information is processed. Practically, connectivity maps can also be used in situations where a particular neuron/neural volume is under study and there is a need to find other connected elements. In this study, we describe the connectivity between compartmentalized brain volumes in the brain of *Drosophila*. Structural analysis identifies the location of information processing hubs, which are densely connected with much of the brain. We also map the location at which different types of sensory information enter the brain. This allows a sensory-based analysis that can be used to generate hypotheses about the putative circuits underlying specific behaviors, which we demonstrate for an antenna mechanosensory-based innate behavior. We propose that a sensory-based analysis performed on a connectivity network may be a constructive approach for understanding behavior in other organisms whose neural connectivity maps are similarly described.

which has been defined as the "macrocircuitry" of a nervous system [19,20]. It is important to distinguish macrocircuitry from microcircuitry, and their relationship to each other. The study of macrocircuitry leads to "wiring diagrams" connecting "functional regions," providing global constraints on how information can flow through the brain. Analysis of such a wiring diagram results in elementary, but indispensable, interpretations of the brain's regions and pathways in the context of sensory and motor functions. However, as has been noted in similar work in sharks [21], the limitations of such a macrocircuitry diagram for basic physiological understanding of the nervous system are significant. Eventually, what will be needed is an understanding of the specific axonal and dendritic innervations of each neuron, the "microcircuitry," including determination of transmitter types, detailed quantification of synapsis with all post-synaptic partners, and other neuroactive phenomena that affect each neuron. However, having a macrocircuitry wiring diagram and the associated interpretations is of great value for microcircuitry approaches. Specifically, such a low resolution map allows for a pre-selection of candidate brain areas for directed microcircuitry-type studies that may not otherwise be evident. In addition, the results from microcircuitry experiments can benefit from the brain-wide context that a macrocircuitry wiring diagram permits.

In this article, we have used data describing the compartments and tracts of the adult CNS [12] combined with corresponding developmental information [22] to construct a macroscopic-level connectivity map of the adult fly brain. The resolution of our map consists of a description of the interconnections between defined neuropile compartments, providing constraints on how information can flow through the central brain. Analysis of network topology and putative functional roles of compartments allow us to measure several network features and compare these to similarly studied vertebrate nervous systems. To investigate the experimental utility of such a map, we predict and experimentally verify a role of the fly's simple eye, the ocelli, on an antenna mechanosensory induced behavior. It is the hope that incorporation of behavioral results like these into the common structured framework of a connectivity network will allow novel and synthetic predictions, an approach that is likely to prove valuable for similar efforts [23] in other model organisms.

Results/Discussion

Functional Relevance of Neuropile Compartments

In the vertebrate brain, the presence of a physical boundary (such as sulci at a macroscopic level, or the glia that comprise the white matter at a subcortical level) between one volume and another is a defining feature of functionally relevant anatomical modules. To determine the level of physical segregation of the anatomically defined compartments of the *Drosophila* brain (abbreviations defined in Table S1) [12], we measured the percent of surface area of each compartment that is covered by glial processes, neurite bundles, and trachea in five individuals (Figure 1; Table 1). We found that surface area coverage ranged between 60.8% and 99.8%. We observed that the compartment surfaces left uncovered are stereotyped, occurring in the same areas in different individuals. This stereotypy suggests that gaps in glial coverage may allow for limited communication between adjacent compartments. We performed a qualitative analysis of the confidence with which each volume has been identified (indicated on Table 1) and found a similar level of confidence to what has been reported for the visual areas of the macaque brain [24]. The antennal lobe (99.1% coverage; yellow in Figure 1), mushroom body (92.0% coverage; pink in Figure 1), and central complex substructures (91.7%–99.8% coverage; green in Figure 1) have a high level of physical isolation. However, the other compartments that have been described as functionally specialized, including the lateral horns (red in Figure 1) and AMMC (blue in Figure 1), have a level of encapsulation that is similar to the remaining anatomically defined compartments (mean 71.3% versus mean 77.6%, respectively). Therefore, we suggest that the remaining anatomically defined compartments may also be functionally specialized.

A Tract-Based Connectivity Map

The fly central brain is formed by approximately 30,000 neurons whose cell bodies are arranged superficially in an outer cortex surrounding an inner neuropile, formed by their neurites (axons and dendrites). The volume of the neuropile is subdivided into structurally defined compartments, some of which have been shown to be specialized functional units (for example, the antenna lobes [15], mushroom bodies [25], and central complex [26]). Information flows between neuropile compartments through neuronal tracts. For example, olfactory information from the antenna lobe is conveyed to the lateral horn through three antenno-cerebral tracts, mACT, oACT, and iACT [27]. The major tracts of the brain can be visualized by immunochemically labeling the adhesion molecules Neuroglian and Fasciclin 2 (Figure 2A; abbreviations [12] defined in Table S2). In these preparations, tracts appear as long cables that *unravel* at their ends as they enter a neuropile compartment.

Comparison of the visualized tracts with previously described examples indicated that immunolabeling did not fully recapitulate the known trajectory of the tract. For example, the inner antenna-cerebral tract (iACT) is formed by interneurons that innervate the antennal lobe, calyx, and lateral horn neuropile compartments [25]. In preparations immunolabeled against Neuroglian (Figure 2A), labeling of the iACT reaches the surface of the antennal lobe and calyx compartments but does not delve inside (Figure 2B). In contrast, the neurite bundle clearly penetrates deeply into the lateral horn compartment. While neuroglian labeling is strong in neuronal tracts, we suspect that the lack of

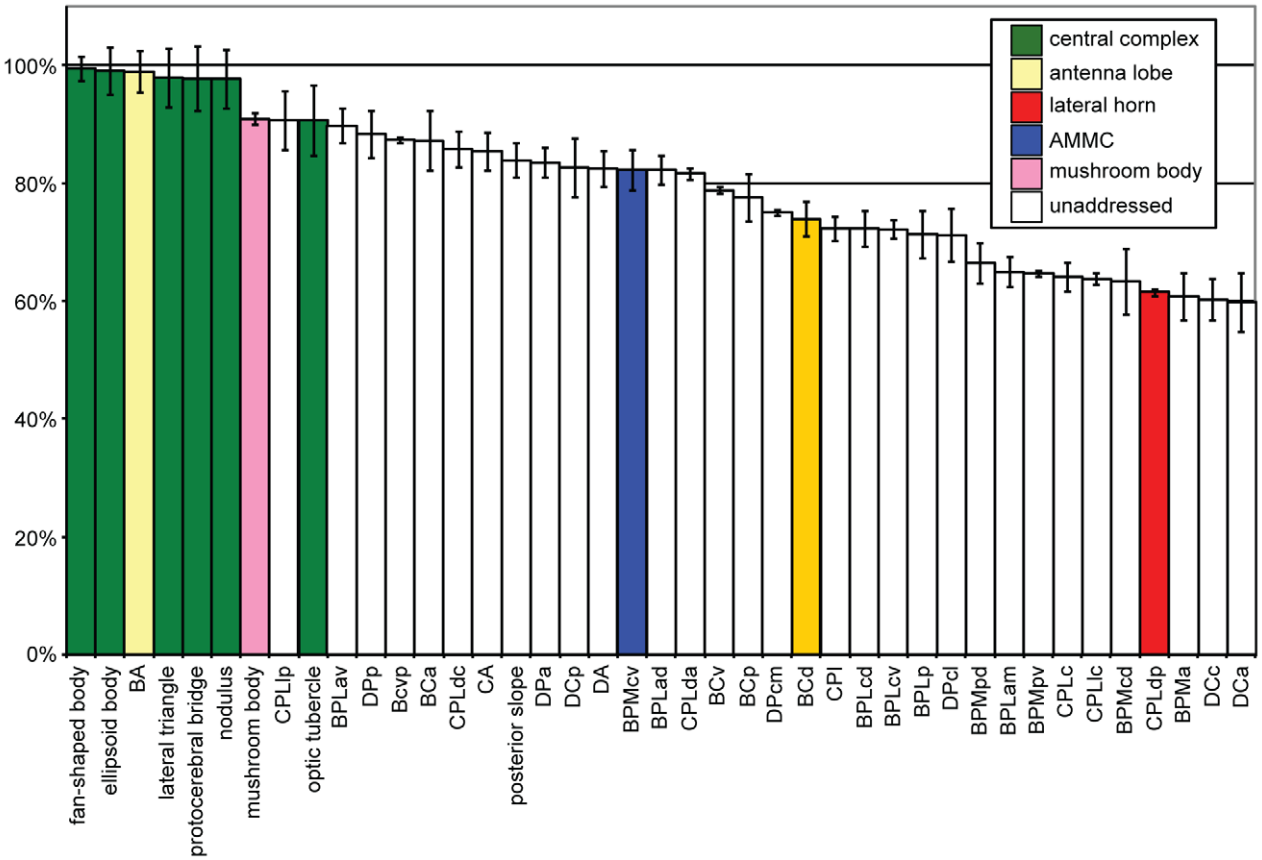

Figure 1. Surface area coverage of neuropile compartments. Histogram showing the percent of surface area occupied by glial sheaths, trachea, or fasciculated neurite bundles for each neuropile compartment. The surface area coverage of each compartment was quantified in five individuals. Groups of compartments are shown in color. Green, central complex substructures; yellow, antennal lobe/BA; red, lateral horn/CPL; blue, AMMC/BPM; pink, mushroom body; hatched, remaining undescribed neuropile compartments. The nomenclature of the neuropile compartments [12] is defined in Table S1. Error bars indicate the S.E.M.
doi:10.1371/journal.pbio.1000583.g001

labeling at the termination point is due to the defasciculation of the neurites from the bundle and the concomitant lack of adhesion molecules between the fibers.

Previous studies have systematically identified and named all the tracts in the adult brain [12], and we have now extended this description to include the neuropile compartments present at the tract termination points (Table S3). As indicated in the table, we found a total of 125 connections between unique compartment pairs, resulting in a total of 480 connections (when counting each connection in both directions and in both left and right hemispheres). We used this set of potential connections between neuropile compartments to construct a connectivity matrix at a neuropile compartment level resolution (Table S4). For the cases in which the tract did not obviously penetrate a neuropile compartment, we conservatively interpreted the tract as potentially terminating in all of the compartments adjacent to the termination point. This approach avoids missing an actual connection (false negative) but likely leads to the introduction of false positives, which we addressed by validating with the independent developmental approach described in the next section. The basis of this interpretation is also consistent with the idea that partially encapsulated adjacent compartments may allow limited inter-compartment communication in the form of neurites that can ramify between multiple compartments without going through fasciculated tracts. As a network, the neuropile compartments comprise the nodes and each tract is a single edge. All edges are undirected in this tract-based network because the anatomical identification of tracts does not provide information about the directionality of information flow through those tracts.

In the above network, the tracts are interpreted as cables connecting the neuropile compartments. We addressed whether the neurites in a neurite bundle interact with the surrounding neuropile as they travel towards their target compartments. Using a Nrv2-Gal4>UAS-GFP line that expresses GFP in cortex and neuropile glial cells, we observed glial sheaths wrapping the Neuroglian-labeled fascicles (Figure 3A), as reported previously [28,29]. Although anecdotal, we did not observe any fascicles that lacked glial ensheathment. This suggests that neurites are physically insulated as they travel through the neuropile. However, the small size of the fascicles (half have a diameter smaller than 4 microns) combined with the relatively coarse axial resolving power of light microscopy did not allow us to conclusively determine the completeness of fascicle encapsulation for all fiber tracts. We therefore used transmission electron microscopy to investigate the ultrastructure along a neurite bundle. In accordance with our observations from light microscopy, we observed a lamellipodia-like glial sheath located at the boundary between the neurites in a bundle and the surrounding neuropile (Figure 3B). In addition, for the three neurite bundles we followed with serial electron micrographs, we did not observe any chemical synapses (presence of a T-bar or vesicle aggregation) or gap junctions between neurites within a fiber bundle and the surrounding

Table 1. Neuropile compartments.

Compartment Name	Synonym	References	Confidence	Physical Encapsulation
BA	Antenna lobe	[25]	1	99.0%
BCa	Ventrolateral protocerebrum		2	87.3%
BCd	Lateral accessory lobe/ventral body		2	74.0%
BCp	Ventrolateral protocerebrum		2	77.6%
BCv	Ventrolateral protocerebrum		2	78.9%
Bcvp	Flange		2	87.4%
BPLad	Ventrolateral protocerebrum		2	82.3%
BPLam	Ventrolateral protocerebrum		3	65.0%
BPLav	Ventrolateral protocerebrum		2	89.8%
BPLcd	Ventrolateral protocerebrum		2	72.3%
BPLcv	Ventrolateral protocerebrum		1	72.2%
BPLp	Posterior lateral protocerebrum/optic glomeruli		3	71.4%
BPMa	Ventral complex		3	60.8%
BPMcd	Ventral complex		3	63.4%
BPMcv	AMMC		2	82.3%
BPMpd	Ventral complex		3	66.5%
BPMpv	Ventral complex		3	64.7%
CA	Crepine		2	85.4%
CPl	Clamp		2	72.4%
CPLc	Clamp		3	64.1%
CPLda	Superior intermediate protocerebrum		2	81.7%
CPLdc	Superior lateral protocerebrum		2	85.8%
CPLdp	Lateral horn		3	61.5%
CPLlc	Superior lateral protocerebrum		2	63.8%
CPLlp	Superior lateral protocerebrum		2	90.7%
DA	Superior medial protocerebrum		2	82.5%
DCa	Superior lateral protocerebrum		3	59.8%
DCc	Superior lateral protocerebrum		3	60.3%
DCp	Superior lateral protocerebrum		2	82.7%
DPa	Superior medial protocerebrum		2	83.6%
DPcl	Superior medial protocerebrum		2	71.3%
DPcm	Superior medial protocerebrum		2	75.2%
DPp	Superior medial protocerebrum		2	88.4%
ellipsoid body	-Same-	[70–73]	1	99.1%
fan-shaped body	-Same-	[71,72,74]	1	99.5%
lateral triangle	Lateral complex bulb	[73]	1	97.9%
mushroom body	-Same-	[75]	1	91.0%
nodulus	-Same-	[76]	1	97.7%
optic tubercle	-Same-	[77] (in locust)	1	90.7%
posterior slope	-Same-	[78]	1	84.0%
protocerebral bridge	-Same-	[72]	1	97.8%

Functionally addressed compartments (volume) = 23%; remaining compartments (volume) = 77%. Various features of the neuropile compartments of the fly central brain (abbreviations are defined in Table S1). ''Synonym'' column provides alternate compartment names as found in the literature. ''Reference'' column refers to predominately recent published reports indicating a specific behavioral effect localized to the indicated neuropile compartment. ''Confidence'' refers to the confidence that a volume has been identified and charted and is rated on a qualitative 4-point scale previously defined for Macaque [24]. The scale ranges from extremely precise (rating 1) to completely nontopographic (rating 4). ''Physical Encapsulation'' refers to the percent of surface area covered by a physical boundary (also see Figure 1). ''Volume'' refers to the total volume, in cubic microns, that each compartment comprises in the fly brain. ''Sensory modality'' refers to the sensory modality that enters the indicated neuropile compartment. Abbreviations: A, ascending; AM, antenna mechanosensory; G, gustatory; H, hygrosensation; PL, polarized light.
doi:10.1371/journal.pbio.1000583.t001

neuropile. In addition, previous reports [12] with preparations labeled with immunomarkers for synaptic proteins (such as Cadherin-N, bruchpilot, or n-synaptobrevin) show these fascicles are essentially unlabeled. Although anecdotal, these findings support the interpretation that neurite bundles are synapse-poor ''cables'' that connect the synapse-rich compartments.

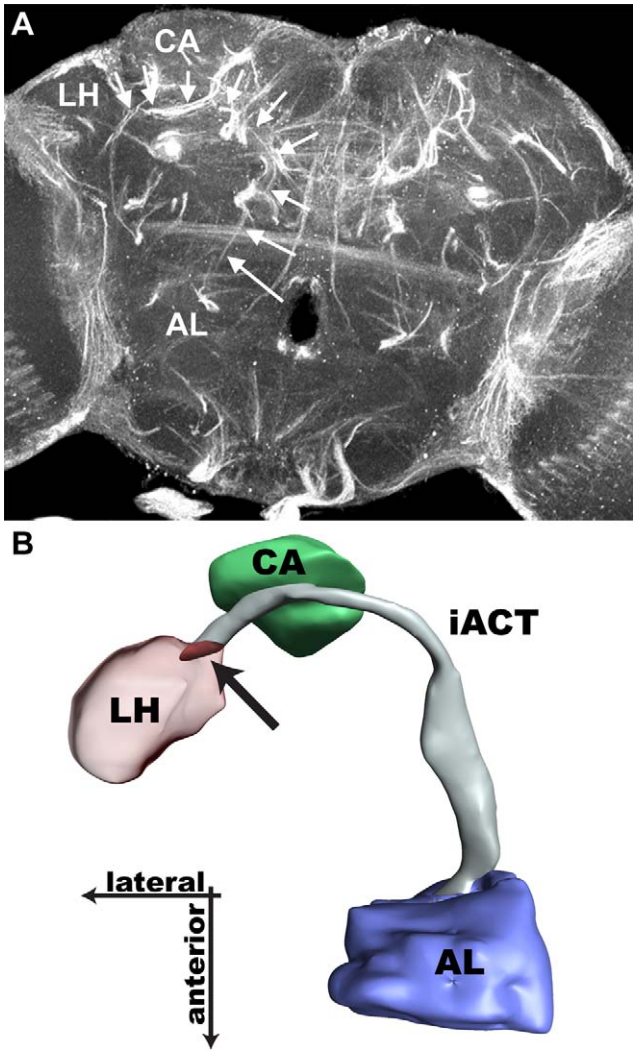

Figure 2. Neuroglian immunolabeling of neurite bundles. (A) Forty micron thick maximum intensity projection section of an adult brain immunolabeled against Nrg. Arrows point to iACT tract visible in the left hemisphere of this section. The iACT tract was manually segmented and used to create a (B) three-dimensional model (shown, for clarity, from a dorsal view). The two tract end-points were segmented as far as were visible in the underlying stack. Note that the iACT tract does not contact the antenna lobe or calyx but can be seen to deeply innervate the lateral horn compartment (arrow). Abbreviations: AL, antenna lobe/BA (show in blue); CA, calyx (shown in green); iACT, inner antennal cerebral tract (shown in grey); LH, lateral horn (shown in transparent red).
doi:10.1371/journal.pbio.1000583.g002

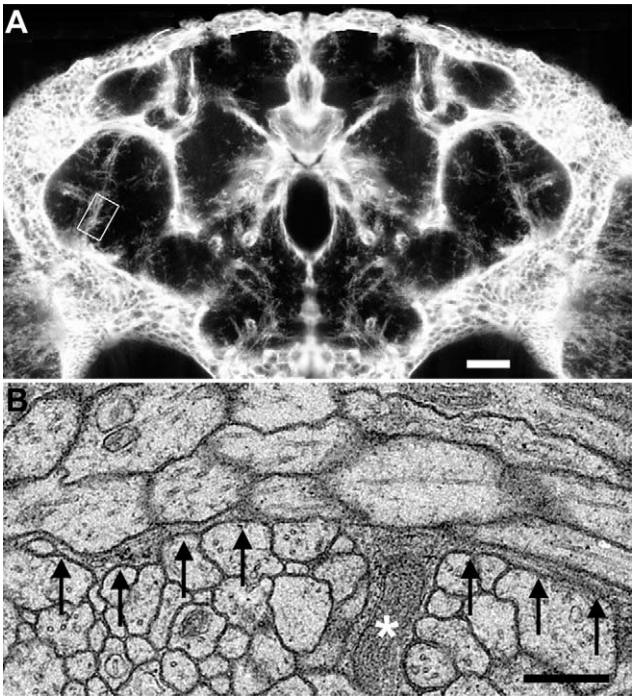

Figure 3. Encapsulation of neurite bundles by glial sheaths. (A) Nervana 2-Gal4 [63] driving expression of GFP shows neuropile glia of the adult brain separating fasciculated neurite bundles and compartments. (B) Transmission electron micrograph of an area within the boxed area shown in (A). The cross-sectional profiles on top represent neurites fasciculated together within a bundle; those on the bottom show neurites in the surrounding neuropile. The soma of a neuropile glia (labeled by an asterisk) wraps the neurite bundle with a membrane sheath (labeled by arrows). No evidence of chemical synapses or gap junctions could be detected between neurites in a fasciculated bundle and the surrounding neuropile. Scale bars: (A) 30 μm; (B) 0.5 μm.
doi:10.1371/journal.pbio.1000583.g003

Tract bifurcations represent an important consideration because our analysis is based on characterization of tracts via a gross morphological marker. Bifurcations visible at a gross level can occur via two mechanisms: (1) branching of some, or all, of the neurites within a bundle (Figure 4A) or (2) a segregation of independent axon bundles (Figure 4B). Knowledge of the specific innervation pattern of each neuron is required for a detailed study of neuronally mediated information encoding, computation, or processing. However, the inability to distinguish the mechanism causing a bifurcation does not hinder analysis at the level of information flow between compartments of the brain. For example, in the case of the olfactory projection neurons in *Drosophila*, which exhibits both types of bifurcations, one can model how information flows accurately without this distinction (Figure 4C). Thus, connections within our connectivity map are accurate in terms of information flow at the compartment level, and thus consistent with the goal of facilitating future work, but additional in-depth experimental work at a microcircuitry level will still be required to resolve how information is processed for any specific connection.

A Developmentally-Based Connectivity Map

Due to our use of an adhesion molecule marker to identify tracts, we suspected that the tract-based approach taken to describing connectivity may be biased against finding connections between adjacent compartments. In order to fill in this gap, we independently generated a model of connectivity based on developmental information.

Recent work has systematically followed the development of neuropile compartments through metamorphosis [12], allowing us to analyze the partially differentiated neurons of the larval brain and infer the adult compartments that they will innervate. In the larva, neurons of each of the approximately 100 lineages extend neurites along with their siblings to form fasciculated bundles that will develop into the adult tracts [12,30]. At stereotypical locations along the bundle, we observe either filopodial tufts or positions in which the bundle partially defasciculates (yellow arrows in Figure 5A,C). As has been reported [31], these positions prefigure the location at which interstitial and terminal arbors will form in

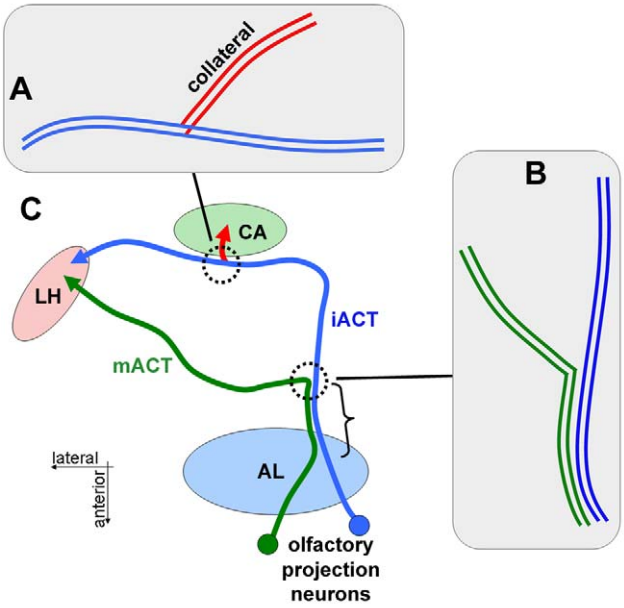

Figure 4. Analysis of neurite bundle bifurcations at a gross morphological level. Schematic of a tract bifurcation as a result of either (A) branching of all neurites \within a bundle or (B) segregation of independent neurites to separate targets. (C) Dorsal-view schematic of two types of olfactory projection neurons that have neurites that project through either the mACT (green) or iACT (blue) tracts to their respective targets. Individual neurites within the iACT branch send a collateral into the calyx as they travel towards the lateral horn (following the mechanism shown in A, upper dashed circle). At a gross morphological level, the proximal portion of the mACT and iACT tract (indicated by the bracket) appears as one entity. Thus, at the position where the mACT breaks from the iACT (indicated by the lower dashed circle), the tract appears to bifurcate (following the mechanism shown in B). Abbreviations: AL, antenna lobe/BA (show in blue); CA, calyx (shown in green); iACT, inner antennal cerebral tract (shown in blue); LH, lateral horn (shown in transparent red); mACT, medial antennal cerebral tract (shown in green).
doi:10.1371/journal.pbio.1000583.g004

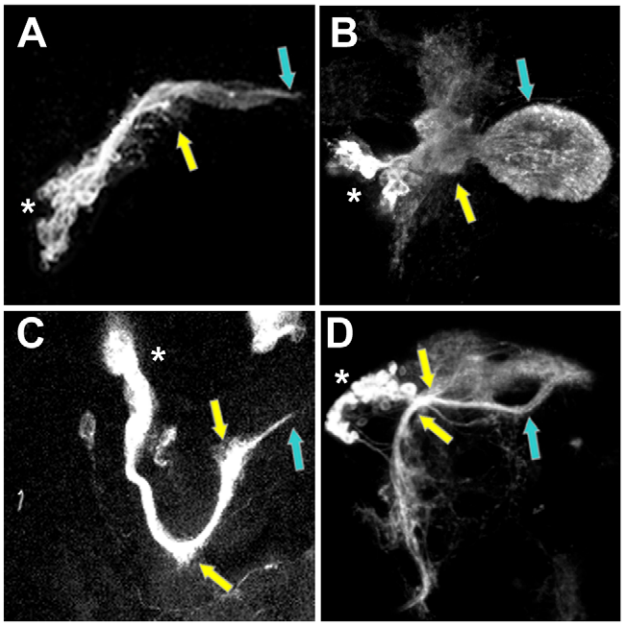

Figure 5. Larval filopodial tufts and bundle defasciculations predict adult arborizations. MARCM clones [66] labeling the (A and B) DALv1 and (C and D) DPLI2 lineage of interneurons. Shown are preparations of the same lineage in a wandering third-instar (A,C) and a different 1–2-d-old adult (B,D) that happened to have the same lineage labeled. Asterisk (*) indicates the position of the lineage cell bodies. In the larva, yellow arrows indicate interstitial positions along the bundle in which filopodial extensions or bundle desfasciculations were observed. The corresponding yellow arrow in the adult lineage indicates the position where terminal arbors have formed from these positions. Blue arrows in the larva indicate position where the neurite bundle terminated. The corresponding position is labeled in the adult with a blue arrow. The adult h1 branch of the DALv2 lineage innervates two compartments: the lateral triangle (prefigured by the defasciculated bundle in the larva) and the ellipsoid body (located at the bundle termination point). The DPLI2 lineage innervates three compartments. Interstitially along the bundle it innervates the DPcl and CPLda compartment (prefigured in the larva (C) by a filopodial extension, left yellow arrow, and bundle defasciculation, right yellow arrow, respectively). In the larva, the bundle terminates in the CPLdp compartment where it will arborize in the adult (D). All brains are oriented so that midline is to the right and dorsal (in the neuraxis) is up.
doi:10.1371/journal.pbio.1000583.g005

the adult as the neurons fully differentiate (Figure 5B,D). We systematically measured these positions for all lineages (Table S5) using a collection of MARCM clones that includes all the central brain lineages in the wandering third-instar larva (Figure S1). We used this information to make putative determinations of which adult neuropile compartments are potentially contacted by each lineage of neurons (Table S5).

While the above model predicts connectivity, we also sought to determine the direction of information flow. Intracellular compartments in *Drosophila* interneurons can be distinguished by features such as microtubule orientation and localization of pre- and post-synaptic sites [32,33]. Analysis of the localization of these cytoskeletal markers in 10 lineages (9.4% of the total population) from these studies as well as our current work (Figure 6; Table 2) indicate that the first interstitial branch position is labeled by cytoskeletal markers that are associated with post-synaptic sites, while the remaining interstitial and terminal positions are labeled by cytoskeletal markers associated with pre-synaptic sites. For the purpose of generating a testable predictive model, we generalized that all arborizations occurring at the first interstitial site are post-synaptic while the remaining arborization points (both interstitial and at the terminal) are pre-synaptic (Table S6). For cases in which there is functional data, these assumptions prove valid (e.g., the olfactory projection neurons and the Kenyon cells of the mushroom body). Note that visualizing the arbors of a differentiated adult neuron would not allow for a conclusive determination of which branches are interstitial and which are terminal because the distance from the originating soma is not a reliable marker (some interstitial branches are long). We rely on our observations of these neurons in their partially differentiated state where we can readily distinguish between the terminal and the interstitial arbors.

We have assumed that all of the connections (edges) in the model have a directionality with proximal input arbors and distal output arbor(s). We are fully aware, though, that many of the input and output arbors will likely contain a mixture of both pre- and post-synaptic sites as has been described in previous Golgi studies [34]. It is useful to look at the vertebrate olfactory system in which mitral cells, which directly receive olfactory information from olfactory receptor neurons and then project to various parts of the brain, have both pre- and post-synaptic endings with granule cells in the olfactory bulb. The mitral cells form excitatory glutamatergic contacts with granule cells. The granule cells then have divergent dendritic arbors that form inhibitory GABAergic synapses with multiple mitral cells, a configuration which is thought to induce lateral inhibition in the neighboring mitral cells

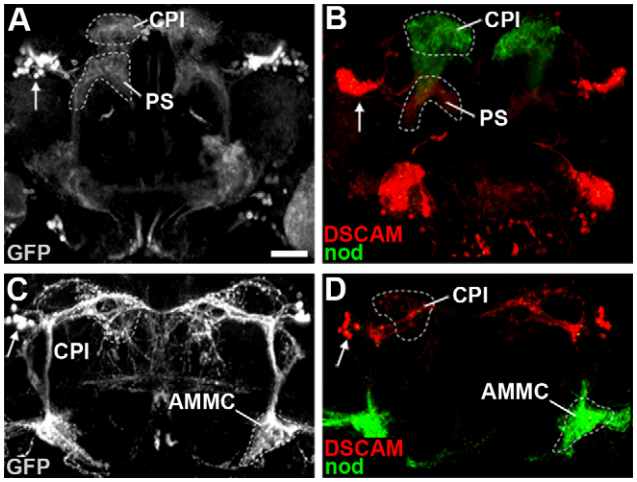

Figure 6. Pre- and post-synaptic enrichment of arborization areas. (A and C) Expression pattern of R18H04 and R29C10 adult-specific driver lines expressed in the BAlp2 and DPLp2 lineages of interneurons, respectively. (B and D) Pre-synaptic sites are visualized by driving expression of DSCAM::GFP, shown in red. Post-synaptic sites are visualized by driving expression of nod::LacZ, shown in green. Arrows indicate position of cell bodies. See Table S1 for abbreviations. Scale bar: 30 μm.
doi:10.1371/journal.pbio.1000583.g006

[35]. In this case, mitral cells have an overall directionality (from olfactory bulb to specific brain targets), while the mixed pre-/post-synaptic endings are important for proper pre-processing of the olfactory information being relayed. For neurons in *Drosophila* that have arbors with mixed pre-/post-synaptic endings, we similarly expect the neuron to have an overall directionality that can be represented at a macro-scopic level, but that local interactions within a compartment could modulate or gate this information flow through the cell. A synaptic-level description of the neurotransmitters present in the mixed arbors of *Drosophila* neurons will be essential for understanding the processing roles of these neurons.

Our current directionality rules allows us to refine the developmentally based model by making edges directional (Table S7). We found a total of 202 unique and directed predicted connections between compartments. Interestingly, 12 of the compartments (22 when counting each compartment in both hemispheres) were predicted to be innervated by intrinsic local interneurons, those that arborize only within a single compartment. Overall, the developmental model predicted a total of 441 edges (when counting each connection in both the left and right hemispheres).

Comparison and Significance of Similarity between Larval and Adult Connectivity Maps

We compared the developmentally derived connectivity model with the tract-based one. Since we suspected that the tract-based approach is biased towards long-distance connections, we initially only compared non-adjacent connections. The tract-derived network has a total of 125 unique non-adjacent connections. Of these, the developmental model predicts all but three edges (BA – CPLdp, BCa – CPLdp, and DCa – contralateral mushroom body). Hence, the developmental model predicts 97.6% of long-range connections that we observed in the adult brain using tract markers. In addition, the developmental model provides unique information about short-range connections between adjacent compartments.

Our finding of a high level of similarity between the larval lineage-based connectivity map and the adult tract-based connectivity map is particularly interesting in the context of the stereotyped pruning mechanism that has been described in vertebrate neurogenesis. In the developing brain, cortical projection neurons often form substantial but transitory collaterals that are removed through a process called stereotyped pruning [36] (for example, occipital cortex neurons form a transitory collateral in the pyramidal tract [37]). If such phenomena were common in the developing *Drosophila* brain, then we would expect that the connectivity observed in the *Drosophila* larval brain would include transitory connections that are not maintained into the adult. However, our finding that 122 of 125 long-range connections are maintained suggests that the secondary neurons in the fly do not undergo stereotyped pruning on a wide scale. A similar lineage-based connectivity map of the ventral CNS that has been reported [38] may provide a comparable approximation of the final adult connectivity of the ventral CNS. In all cases, a detailed anatomical analysis of the neurons within each lineage through metamorpho-

Table 2. Evidence of pre- and post-synaptic enrichment.

Lineage	Gal4 Driver Used	Pre-Synaptic Cytoskeletal Marker	Post-Synaptic Cytoskeletal Marker	Reference	Figure
BAlp2	R18H04	tau::LacZ	DSCAM::GFP	*Ibid.*	6a,b
BAla1	GH146	tau::GFP	nod::YFP	[33]	3
BAla2	GH146	tau::GFP	nod::YFP	[33]	3
BAmv3	GH146	tau::GFP	nod::YFP	[33]	3
BLD5	ato	nSyb::GFP	DSCAM::GFP	[32]	2d–f
DPLp2	R29C10	tau::LacZ	DSCAM::GFP	*Ibid.*	6c,d
Mb1	OK107	tau::GFP	nod::YFP	[33]	2
Mb2	OK107	tau::GFP	nod::YFP	[33]	2
Mb3	OK107	tau::GFP	nod::YFP	[33]	2
Mb4	OK107	tau::GFP	nod::YFP	[33]	2

List of 10 lineages of interneurons in which the differential cytoskeletal arrangement of the arborizations have been experimentally addressed using the indicated driver lines. This is a comprehensive list of lineages that are currently genetically addressable. "Reference" and "Figure" columns refer to published reports, in which the indicated cytoskeletal markers were used to determine putative pre- and post-synaptic sites.
doi:10.1371/journal.pbio.1000583.t002

sis will be required to conclusively determine the actual level of pruning that occurs. It is important to note that we are limiting our description to the larval-born secondary neurons. The adult fly brain contains a small number of embryonic-born primary neurons (<5%), which have been described to survive into the adult after undergoing significant pruning and remodeling [39,40].

Creating a Final Connectivity Map through Consensus

We next generated a consensus connectivity map from the two independent approaches, taking into account suspected biases, in order to reduce the number of false positives that may be present in either source. Given the suspected bias of the structural markers, we divided the inter-compartmental connections into two categories based on whether they connect adjacent neuropile compartments. For the adjacent connections, we accepted the connection as a valid consensus connection if it is a valid connection in the developmentally predicted model alone (as explained in the previous section). For the non-adjacent connections, we accepted the connection as a valid consensus connection if and only if it is present in both the tract-based and developmental connectivity maps. Overall, this approach was designed to help reduce the number of false positives that may be present in either dataset. We followed these rules in generating a consensus network by combining the developmentally predicted network and the tract derived network (Figure 7; Table S8). The consensus network consists of 155 unique connections (resulting in a total of 339 individual connections). Overall, 26% (40 out of 155) of connections are commissural and 23% (36 connections) involve the central complex. Of the remaining 79 ipsilateral connections, 15% (12 connections) remain within a single compartment, while the final 88% (70 connections) connect different ipsilateral compartments.

Anecdotal Validation of the Connectivity Map

Ideally, we would assess the validity of the connectivity map by corroboration with comprehensive experimental data. Because such a comprehensive dataset does not exist, we took three approaches to validate the proposed connections. First, the high level of similarity between the two independently derived connectivity maps (97.6% of non-adjacent connections match) suggests that each method is reliably characterizing the underlying biological system. Second, we searched the literature and attempted to address which connections have been experimentally addressed in the adult *Drosophila* brain ("Reference" column in Table S3). Overall, we were able to find evidence for 10 of the 339 putative connections (2.9%). We did not find any examples of a known connection that was not captured by our network. We believe that the low number of validated connections is symptomatic of the fact that fly neurobiology has focused experimental effort on a relatively small portion of the brain. The final method of validation involved behaviorally testing the presence of connections with the goal of assessing the predictive power of such a map for guiding experiments, described below. These behavioral experiments provide evidence for two additional unique connections that, bilaterally, represent four total connections. Thus, overall we are able to find evidence supporting 14 of the 339 putative connections (4.1%). We expect that the newly described connections will be equally valid.

Topologically Based Analysis of the Connectivity Map

Knowledge of the compartmental connectivity network is insufficient for understanding how the nervous system functions in detail. However, theoretical work in systems such as C. elegans [41], cat cerebral cortex [42], and the macaque cortex [43] has

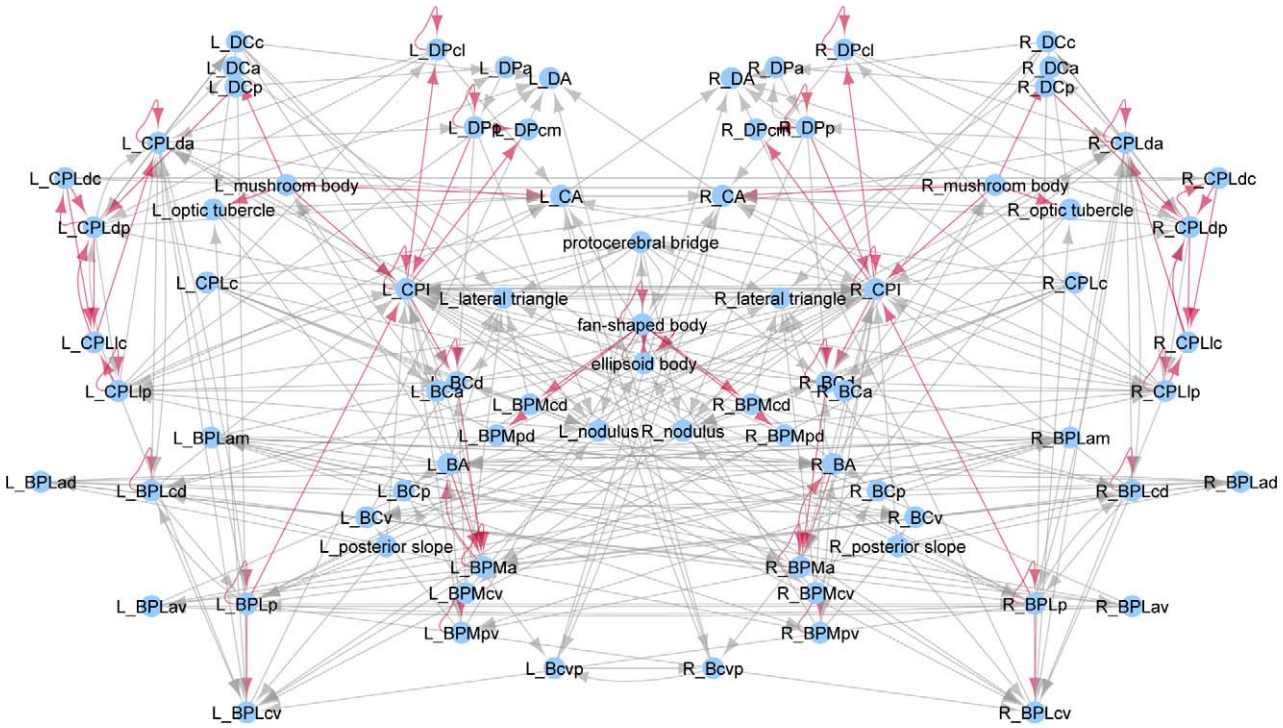

Figure 7. The *Drosophila* whole-brain connectivity network. The nodes (blue circle) in the network represent the neuropile compartments of the brain. The edges (or connections) between the nodes represent putative connections, based on the consensus logic, that are derived from structurally observable bundles and developmental predictions from the lineages of neurons that form the brain. Edges shown in red are adjacent connections predicted by the developmental model but not supported by tract-based evidence. Nodes are located in approximately the same position as the center-of-mass positions of the compartments in situ. Edges are based on the connectivity matrix in Table S8.
doi:10.1371/journal.pbio.1000583.g007

demonstrated the value of performing complex network analysis to determine general properties of networks such as those described by anatomical connectivity datasets [44]. We looked at the following five properties of the adult *Drosophila* central brain network using metrics that have been defined elsewhere [44]: integrative ability, clustering, small-worldness, resilience, and centrality. Comparisons, where appropriate, were made to a topologically random directed network that was matched for number of nodes, edges, and in/out degrees. All analyses were done using directed binary networks.

We first analyzed metrics to assess the potential for functional segregation, which is typically measured via the presence of clusters [44]. Clusters in this context are groups of compartments that are densely interconnected and may be involved in specialized processing of information. The mean clustering coefficient is a metric used to measure the extent that nodes in a graph tend to cluster together and is meaningfully compared to a matched random network [45]. We found that the *Drosophila* central brain consensus network has a mean clustering coefficient of 0.335, whereas the matched random network had a mean clustering coefficient of 0.096. Thus, the compartment-level connectivity in the *Drosophila* network shows, on average, a high prevalence of clustered connectivity around individual nodes compared to a random network. The cat and macaque networks show a similar pattern of strong clustered connectivity around individual nodes (0.28 versus 0.05 for the C. elegans network and matched random network, respectively [45]; 0.587 versus 0.423 for the cat cortex and matched random network, respectively; 0.471 versus 0.239 for the macaque cortex and matched random network, respectively). We also computed more sophisticated measures of segregation using a topological community finding algorithm that attempts to divide the given directed network into consistent modules using optimization techniques [44,46]. Based on this analysis, we found that the fly network can be more clearly subdivided into these topologically defined clusters than a matched random network (modularity score: 0.453 versus 0.269, respectively). We applied the same community finding algorithm on the cat and macaque networks and found that these networks also show better topological organization compared to their matched random networks (modularity score: 0.292 versus 0.097 for the cat cortex and matched random network, respectively; 0.378 versus 0.142 for the macaque cortex and matched random network, respectively).

The notion of a small world network, in which a node can reach any other node by a small number of connection steps despite not being neighbors with most other nodes, is thought to represent an anatomical trade-off between integration and segregation and has been described for many other connectivity networks including the cat and the macaque cortex [47,48]. A network must meet two criteria to be defined as a small world [44,45]. First, as we show above, the network must be significantly more clustered than a matched random network. Second, the network must have a similar "characteristic path length," which is an estimate of the average shortest route between any arbitrary pair of compartments, as a matched random network. We found that information must cross through 3.4 intercompartmental connections to travel between any pair of compartments. This number is substantially the same as the characteristic path length of the degree-matched directed random network, 2.95. It is important to note that the characteristic path length varies logarithmically with graph parameters, such as the number of nodes [45], such that large changes in network topology may only have a small impact on this metric. Therefore, this metric must be carefully interpreted outside a small world context. The C. elegans, cat, and macaque networks have similar characteristic path lengths to their respective matched random networks (2.65 versus 2.25 for C. elegans network and matched random network, respectively [45]; 1.77 versus 1.68 for the cat cortex and matched random network, respectively; 2.3 versus 2.03 for the macaque cortex and matched random network, respectively). Overall, we conclude that the *Drosophila* compartmental network meets both criteria and can be described as a small world network. This suggests that the compartment-level architecture of the fly brain is composed of functionally specialized modules interconnected by intermodular links.

Complex network analysis also provides several metrics to indirectly measure resiliency—the anatomical capacity of a network to withstand lesions. One popular measure of resilience is the assortativity coefficient [49]. The assortativity coefficient is a correlation coefficient between the degrees of all nodes on opposite sides of a link. A network with a positive assortativity coefficient is likely to have an interconnected resilient core, while a negative assortativity coefficient suggests the network is likely to be more vulnerable to lesions [44]. For the *Drosophila* compartment-level network, the assortativity coefficient is 0.141 and is therefore likely to have a resilient core of mutually inter-connected high-degree hubs. The assortativity coefficient for the matched random network is -0.034, indicating that the fly connectivity network is structured in a way that is comparatively more resilient than a matched random network. The same analysis applied to cat (assortativity coefficient for cat network: 0.016; for matched random network: -0.133) and macaque (assortativity coefficient for macaque network: 0.024; for matched random network: -0.063) brain networks shows that these vertebrate brain networks are similarly structured to be resilient to lesions.

We next analyzed several metrics for each neuropile compartment to assess the potential importance of each compartment for facilitating integration and resilience. The underlying premise is that the important neuropile compartments often interact with many other regions, facilitate functional integration, and play a key role in network's resilience to perturbations or lesions. The most common measure of centrality is to measure the number of inward and outward connections, or degree, for each node. Analysis of both in-degree and out-degree for all neuropile compartments (Table 3) indicates that the centro-posterior intermediate (CPI) compartment has both the highest in and the highest out degree. Another measure of centrality, betweenness centrality [50], takes the collection of shortest paths between each pair of neuropile compartments and counts the fraction of these shortest paths in which each compartment is present. We computed betweenness centrality (Table 3) and found that the CPI compartment is present in approximately one-quarter of the shortest paths. This indicates that the CPI compartment is likely a key bridging node that connects disparate parts of the network. Interestingly, the next three highest neuropile compartments with high betweenness centrality scores (ellipsoid body, fan-shaped body, and protocerebral bridge) are substructures of the central complex.

Sensory-Based Analysis of the Connectivity Map

The fly's central brain receives information from various sensory modalities (entering through discrete nerves or the cervical connective), which it compares to produce integrated responses. The neuropile compartments innervated by several modalities have been described and we have annotated the network to include information from eight of these (gustatory [51], ocelli: p.154–155 in [34], ascending [52], polarization of light [53], compound eye [54], olfactory [55], hygrosensation [56], antenna mechanosensory [16,17]), which are indicated in Table 1. This

Table 3. Centrality metrics of the *Drosophila* consensus network.

Neuropile Compartment	In-Degree	Out-Degree	Betweenness Centrality
BA	5	5	2.7%
BCa	1	2	1.4%
BCd	8	2	1.1%
BCp	2	2	3.0%
BCv	4	1	0.2%
Bcvp	3	4	0.4%
BPLad	3	8	2.7%
BPLam	2	4	0.3%
BPLav	6	4	0.3%
BPLcd	9	3	2.5%
BPLcv	5	9	1.7%
BPLp	6	3	2.6%
BPMa	1	4	0.6%
BPMcd	1	4	3.4%
BPMcv	1	4	0.7%
BPMpd	3	3	1.4%
BPMpv	3	3	0.2%
CA	9	3	1.3%
CPI	**16**	**16**	**25.3%**
CPLc	0	7	0.0%
CPLda	9	8	5.8%
CPLdc	2	3	0.7%
CPLdp	7	7	3.2%
CPLlc	3	2	0.2%
CPLlp	5	10	4.2%
DA	6	0	0.0%
DCa	2	1	0.3%
DCc	3	5	1.5%
DCp	0	2	0.0%
DPa	2	1	0.2%
DPcl	2	3	0.0%
DPcm	2	0	0.0%
DPp	2	5	2.2%
Ellipsoid body	8	1	6.3%
Fan-shaped body	2	6	9.1%
Lateral triangle	7	1	4.0%
Mushroom body	2	4	1.2%
Nodulus	7	1	0.4%
Optic tubercle	3	3	1.7%
Posterior slope	0	3	0.0%
Protocerebral bridge	3	10	7.4%

The in-degree, out-degree, and betweenness centrality metrics were calculated for each neuropile compartment. The row corresponding to the CPI neuropile compartment is emphasized as it is the maxima of each of the three metrics.
doi:10.1371/journal.pbio.1000583.t003

effort represents a similar but systematic refinement of a sensory-based approach taken in *Musca domestica* [34].

In order to better characterize how sensory information is processed within the connectivity network, we next clustered together compartments based on the similarity of sensory information that they receive. Given the characterization of compartments innervated by several modalities (as described earlier), we computed, for each compartment, the number of connections each modality has to travel through to arrive at that compartment. This resulted in an eight-dimensional feature vector for every node (corresponding to the eight sensory modalities we characterized). Using Euclidean distance between these feature vectors as a measure of affinity between compartments, we grouped the neuropile compartments into clusters using affinity propagation algorithm that operates on directed network graphs [57]. We biased the affinity propagation algorithm such that it over-segmented the network. We then further refined the initial clusters using the following heuristics: (i) merged clusters that were directly receiving the same modality, (ii) merged clusters to make the organization symmetrical, (iii) merged central complex compartments together, and (iv) merged clusters containing only subdivisions of a single larger compartment (two such cases encountered). After applying these criteria to the initial set of clusters, we ended up with 11 clusters of compartments that we called "integration domains" (Figure 8). Analysis of the resulting connectivity between these integration domains provides a high-level look at how sensory information is processed, including the specific sites where different modalities are first integrated (Figure 9). Through this reduced representation, we found that the central complex and antenna mechanosensory integration domains are the most central clusters in the context of sensory processing and integration.

It is useful to look at one of the integration domains in detail to demonstrate the specific types of relationships that lead to neuropile compartments being assigned to the same integration domain. We focus here on the antenna-mechanosensory integration domain since we make use of this domain in our behavioral experiments. This integration domain consists of five neuropile compartments: BPLp, BPMa, BPMcv, BPMpd, and the CPI. The affinity propagation algorithm grouped the BPMa and BPMcv into one cluster (cluster 1) and the BPLp, BPMpd and CPI into another (cluster 2). These two clusters were then joined together because the BPLp, BPMa, BPMcv, and BPMpd all directly receive antenna mechanosensory input, as described in the first refinement step above, resulting in the final antenna-mechanosensory domain. In this case, the CPI compartment is part of this integration domain even though it does not directly receive antenna mechanosensory input because it was originally grouped with compartments that do. Taking a more detailed look at the compartments that were algorithmically grouped into this domain, we find that these compartments share reciprocal connections, including connections bilaterally. This indicates that the CPI compartment requires only one connection and is reciprocally connected with the compartment that directly receives the sensory information. Overall, the antenna-mechanosensory integration domain is a representative case and the compartments in the other integration domains were grouped similarly.

Utility of the Connectivity Map

We next tried to assess how a map along with the relevant sensory information could be practically used for gaining a foothold into the functionally uncharacterized parts of the brain. Because of the compartment-level resolution of the map, we should be able to infer the modalities of sensory information being processed by particular groups of neurons that innervate a neuropile compartment and to identify the compartments in which sensory integration events occur. To do this, we systematically analyzed the sensory-annotated connectivity map

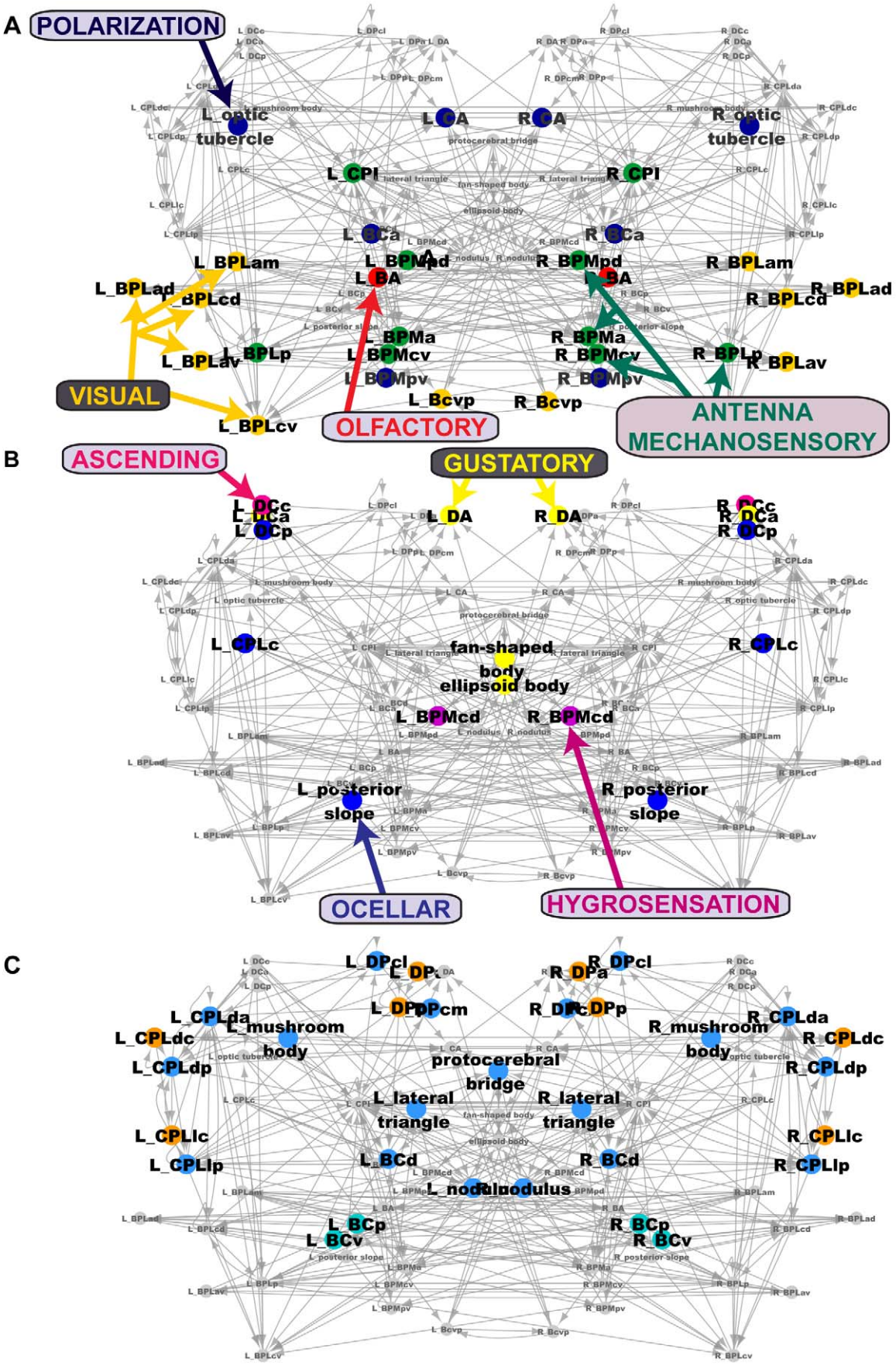
A
POLARIZATION
L_optic tubercle
R_optic tubercle
L_CA
R_CA
protocerebral bridge
L_CPI
R_CPI
L_BPLam
L_BPLad
L_BPLcd
L_BPLav
L_BPLp
L_BPMa
L_BPMcv
L_BPMpv
L_Bcvp
L_BPLcv
R_BPMpd
R_BPLam
R_BPLad
R_BPLcd
R_BPMa
R_BPMcv
R_BPLp
R_BPLav
R_BPMpv
R_Bcvp
VISUAL
OLFACTORY
ANTENNA MECHANOSENSORY
B
ASCENDING
GUSTATORY
L_DCc
L_DCa
L_DCp
L_DA
R_DA
R_DCc
R_DCa
R_DCp
L_CPLc
fan-shaped body
ellipsoid body
R_CPLc
L_BPMcd
R_BPMcd
L_posterior slope
R_posterior slope
OCELLAR
HYGROSENSATION
C
L_DPcl
L_DPa
R_DPcl
R_DPa
L_DPpPcm
R_DPpPcm
L_CPLda
L_mushroom body
L_CPLdc
L_CPLdp
protocerebral bridge
L_lateral triangle
R_lateral triangle
R_CPLda
R_mushroom body
R_CPLdc
R_CPLdp
L_CPLlc
L_CPLlp
L_BCd
R_BCd
L_nodulus
R_nodulus
L_BCp
L_BCv
R_BCp
R_BCv
R_CPLlc
R_CPLlp

Figure 8. Integration domains of the *Drosophila* brain. Connectivity network shown in three panels in which compartments belonging to each of the 11 integration domains are shown in different colors. (A) Olfactory (red), antenna mechanosensory (green), visual (tan), polarization (light purple); (B) ocellar (dark blue), gustatory (yellow), ascending (pink), and hygrosensation (dark purple); (C) lateral accessory lobe (cyan), superior protocerebrum (orange), and central complex (light blue). The three integration domains in (C) do not directly receive any sensory information. The antenna mechanosensory integration domain contains the BPLp, BPMa, BPMcv, BPMpd, and CPI neuropile compartments. The ascending integration domain (which includes input from the SOG) contains the DCc neuropile compartment. The central complex integration domain contains the BCd, CPLda, CPLdp, CPLlp, DPcl, DPcm, lateral triangle, mushroom body, nodulus, and the protocerebral bridge. The gustatory integration domain contains the DA and DCa compartments. The hygrosensation integration domain contains the BPMcd compartment. The lateral accessory lobe integration domain contains the BCp and BCv neuropile compartments. The ocellar integration domain contains the CPLc, DCp, and posterior slope. The olfactory integration domain contains just the BA (antenna lobe). The polarized light integration domain contains the BCa, BPMpv, CA, ellipsoid body, fan-shaped body, and the optic tubercle. The superior protocerebrum integration domain contains the CPLdc, CPLlc, DPa, and the DPp neuropile compartment. The visual (optic glomeruli) integration domain contains the Bcvp, BPLad, BPLam, BPLav, BPLcd, and the BPLcv neuropile compartments.
doi:10.1371/journal.pbio.1000583.g008

to identify the neuropile compartments in which information from each pair of sensory modalities first converge (Table 4).

To demonstrate the utility of a compartmental map, we examined the behavioral integration of antenna mechanosensory and ocellar sensory inputs (bolded on Table 4). We first tried to confirm the map-based prediction that input from the ocelli may modulate antenna mechanosensory information (as indicated on Table 4, other potential sensory integration events can be targeted with currently available driver lines). To do this, we modified an existing assay [16,17] such that we mechanically probed the antenna and observed whether the fly moved either foreleg in response, which we termed the antenna foreleg response (AFR; see Materials and Methods). As predicted, we found that light levels influenced (in this case, decreased) the rate of the antenna foreleg response (Figure 10A). We examined whether the visual stimulus was processed through the compound eyes or the ocelli by selectively blocking input to each one using either genetic methods or by blocking light through the application of a black pigment (Figure 10B and C, respectively). Genetic targeting of the ocellar interneurons was performed using the line R29H12 that was identified by screening through a database of adult brain expression patterns of 4,147 Gal4 lines (Rubin et al., unpublished) that had been constructed as described [18]. We found that input through the ocelli, and not through the compound eye, is necessary for the observed modulation. These results experimentally demonstrate that ocelli in *Drosophila* supply ambient light level information to the CNS, in addition to their suggested role in flight control [58].

The connectivity network indicates several potential circuits through which information from the ocelli can be transduced to the BPMcv (AMMC). Our topological analysis allows us to rank-order these based on centrality and suggests that the circuit mediated by the DPLp2 lineage of interneurons, which arborizes in the CPI compartment and the posterior slope, as a potentially dominant pathway for this information. We used this information as a search image to screen through the expression pattern database. We found three lines (R29C10, R30E08, and R31A06) that drive expression in neurons of the DPLp2 lineage and connect the CPI to the contralateral BPMcv (AMMC) compartment (Figure S2). Based off of gross morphological analysis, the three lines are sparse (<50 neurons) and only intersect in the nine interneurons of the DPLp2 lineage. We thus performed all

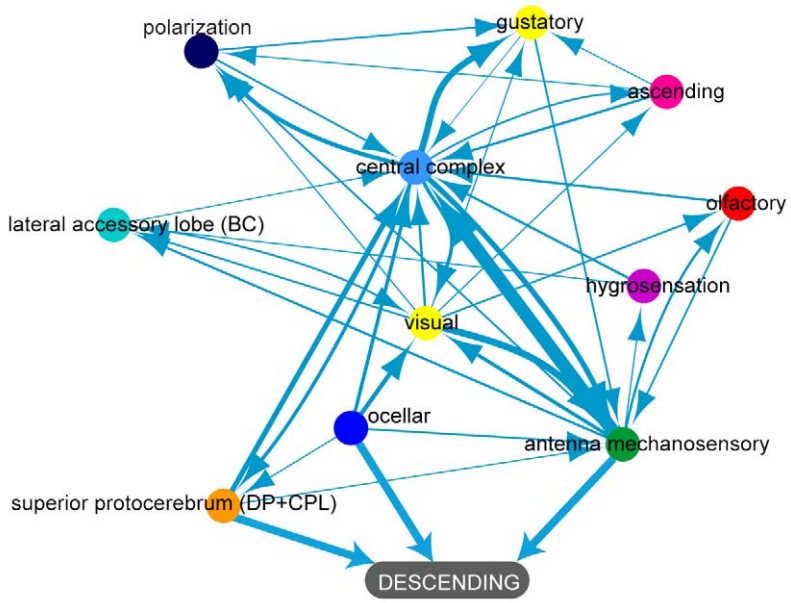

Figure 9. Schematic of sensory integration in the fly brain. Neuropile compartments from the same integration domains were reduced to single nodes (the colors of the integration domains corresponds to those shown in Figure 8). This allows a reduced visualization of how sensory information may flow in the overall network. The width of the connections (edge weights) is based on the number of connections between the underlying compartments within each cluster. Two integration domains (lateral accessory lobe and superior protocerebrum) do not directly receive sensory inputs.
doi:10.1371/journal.pbio.1000583.g009

Table 4. Experimental tractability of sensory integration points.

Pair of Modalities Being Integrated	Compartment(s)	# of Connections	Driver Line(s)
Gustatory - ascending from VNC	DA	1	
Visual - gustatory	DA	1	
Antenna mechanosensory - visual	BPLcd/BPLp/BPMpd	1	
Polarization - ascending from VNC	Optic tubercle	1	
Olfactory - antenna mechanosensory	BA/BPLp	1	
Visual - ascending from VNC	DCc	1	
Visual - ocellar	BPLav/BPLcd	1	
Olfactory - visual	BA	1	
Visual - polarization	Optic tubercle	1	
Antenna mechanosensory - ocellar	**CPI/BPLcd/BPLp/BPMpd**	**2**	**R29C10/R30E08/R31A06**
Antenna mechanosensory - polarization	CA/optic tubercle	2	
Olfactory - polarization	Optic tubercle	2	
Olfactory - hygrosensation	BPMcd/lateral triangle	2	
Antenna mechanosensory - ascending from VNC	BCd/BPLp/DCc/lateraltriangle/nodulus	2	
Ascending from VNC - hygrosensation	BCd/lateral triangle/nodulus	2	
Antenna mechanosensory - gustatory	DA	2	
Olfactory - ocellar	CPI	2	R29C10/R30E08/R31A06
Ocellar - gustatory	DA	2	
Olfactory - gustatory	DA/DCa	2	
Polarization - gustatory	DA	2	
Visual - hygrosensation	BPLad/BPMcd/Bcvp	2	
Ocellar - ascending from VNC	DCc	2	
Olfactory - ascending from VNC	Lateral triangle	2	
Antenna mechanosensory - hygrosensation	BCd/BCp/BPLp/BPMcd/lateral triangle/nodulus	2	
Polarization - ocellar	Optic tubercle	2	
Gustatory - hygrosensation	Ellipsoid body	3	
Polarization - hygrosensation	BCd/BPMcd/CA/nodulus/optic tubercle	4	

List of the 27 integration pairs for each of the eight sensory modalities that were annotated onto the connectivity network. "Compartment(s)" column refers to the neuropile compartment(s) in which the integration of the two sensory modalities first occurs. "# of connections" column refers to the number of network connections that need to be taken before the sensory modality information is integrated at the indicated neuropile compartment. - "Driver line(s)" column refers to driver lines used in this study to target the interneurons that the map indicates are involved with the respective sensory integration event.

doi:10.1371/journal.pbio.1000583.t004

behavioral tests on all three lines in order to demonstrate that the elicited response was caused by these nine intersecting neurons.

We next performed perturbation experiments using the three driver lines to test the network prediction that the DPLp2 interneurons are responsible for integrating light level information from the ocelli with antenna mechanosensory information (Figure 11). As expected, expression of shibire^{ts1} [59] at a restrictive temperature of 32°C with each of the three drivers resulted in normal AFR rates in bright light conditions. However, under low light conditions, the AFR levels were also the same as those seen under bright light conditions (Figure 11A,B). These data indicate that activity in the DPLp2 interneurons is necessary for the ocelli-mediated reduction in AFR. Conversely, AFR rates in flies with expression of dTrpA1 [60] in these neurons at 32°C were similar to controls under low light conditions but had a significantly decreased AFR rate in bright light conditions (Figure 11C,D), which was statistically similar to AFR rates under low light conditions. This indicates that ectopic activity in the DPLp2 interneurons is sufficient to recapitulate the decreased response rate in low stimulus conditions. These two lines of evidence showing the necessity and sufficiency of activity within the DPLp2 neurons support the map-based behavioral prediction of ocellar integration with antenna mechanosensory input. In addition, the context provided by the whole-brain connectivity map (Figure 12) indicates that activity in these interneurons acts to invert the light response received from the ocelli. This suggests the presence of an inhibitory element in the putative circuit.

As discussed so far, we demonstrated how a compartment-level connectivity map can be used to predict the modality of sensory information being processed by a set of neurons based on the innervation pattern of the neurons. It is instructive to look at other systems that have been described at an analogously coarse level and see how else such a map can be successfully used. Felleman and van Essen [24] compiled a compartmental connectivity map describing 305 connections between 32 visual and visual-association areas of the macaque visual cortex. In subsequent papers, this macaque connectivity map played a fundamental role in both experimental design and data interpretation. For example, Schmolesky et al. [61] used the map to predict that the onset of visually evoked stimuli would have a slower response latency in hierarchically "higher" areas (putatively receiving more processed information) than "lower" areas. Using single unit recordings, they assayed eight of the areas and found both response times that were compatible with the anatomical map, as well as some that were not

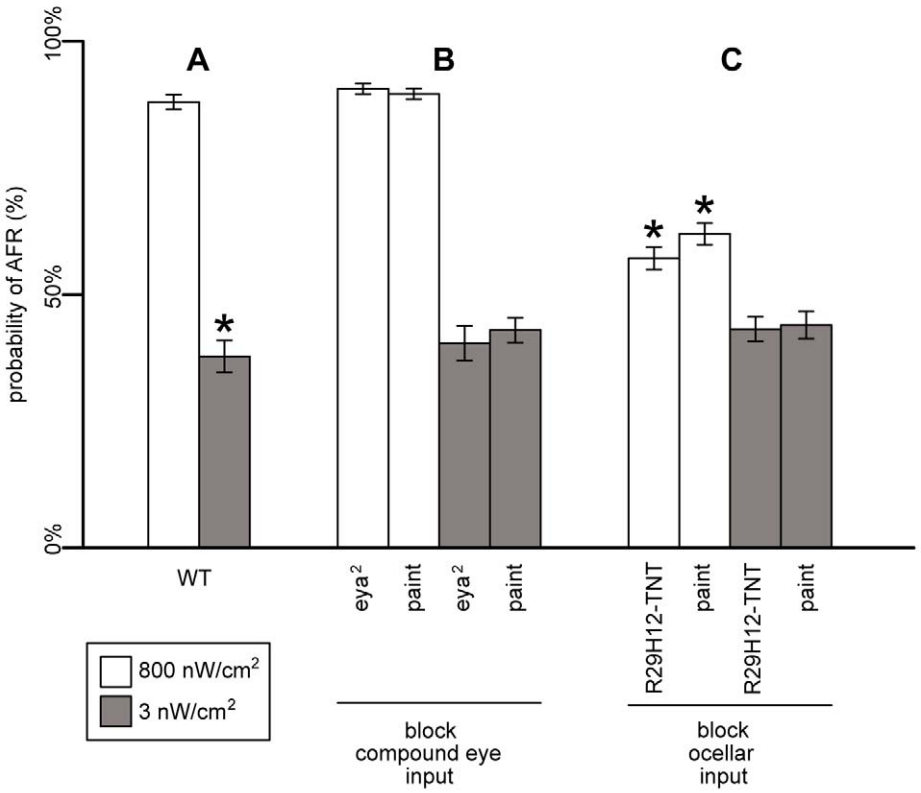

Figure 10. Ambient light levels through ocelli modulate AFR. AFR rates for (A) wild-type flies, (B) flies in which compound eye input/processing has been blocked, and (C) flies in which ocellar input/processing has been blocked under both light (800 nW/cm^2) or dark (3 nW/cm^2) conditions. The compound eye was genetically removed using the *eyes absent* mutant, eya^2. Information from the ocelli to the central brain was blocked by driving tetanus toxin in ocellar interneurons using an ocellar interneuron driver line (R29H12; see Materials and Methods and Figure S2). For each condition, five flies were measured for 100 trials and AFR rates were scored as described in Materials and Methods. Error bars indicate standard error of the means. Asterisks indicate a significant decrease ($p<0.05$ as measured by the chi-square test) in (A) AFR rates in the dark compared to light for wild-type flies and (C) AFR rates of flies in light condition that have ocellar input/processing blocked.
doi:10.1371/journal.pbio.1000583.g010

(such as the FEF at level 8 having, in some cases, the same response latency as V1, from level 1). This work indicates both the value of starting from an anatomical map as well as the need for functional analysis as a requirement for addressing questions of information processing. The macaque connectivity map is also used to help interpret results. Tootell et al. [62] used fMRI to investigate the waterfall visual illusion, in humans, in which stationary objects appear to be moving after prolonged viewing of a stimulus moving in one direction. They found a significant activation in the MT (also known as V5), an area that preferentially responds to motion, when subjects reported illusory motion. Surprisingly, they also found similar, but smaller, activations in two other areas (V2 and V3a) that have not been described to preferentially respond to moving stimuli. This unexpected result was partly explained by the observation that the macaque connectivity map indicates the presence of reciprocal connections between MT, V2, and V3a. We expect that the connectivity map described here for *Drosophila* could be used in a comparable way to both make experimentally addressable questions (as we show above) as well as to help interpret results in the context of known anatomical connections.

Conclusion

This macroconnectivity map provides the first comprehensive analysis of compartment-level connectivity within the brain of *Drosophila melanogaster*, one of the premiere model systems for unraveling the genetic basis of brain connectivity. The map generates testable hypotheses of the sensory processing roles for each of the compartments, including those that have not yet been functionally described (which together constitute the majority of the brain). We demonstrated how a coarse-level map facilitates the identification of neurons involved in processing information from a particular pair of sensory modalities. The identification of a small subset of neurons with a particular functional role is a prerequisite step to the experimental descriptions required of a microcircuitry approach, such as identifying the pertinent neurotransmitters or describing the distribution of synapse with pre- and post-synaptic partners. In addition, the availability of a comprehensive map with the associated sensory information permits functional interpretations in the context of the whole brain. Specifically, the sensory modalities that may send information to these neurons can be systematically tested, along with the corresponding neurons located upstream and downstream in a putative circuit.

In addition, we established that the premetamorphic morphologies of neurons in the larval brain can be used to accurately predict the final adult connectivity network. This finding opens up a new avenue of approaching a subset of questions about adult connectivity by manipulating and observing neurons during larval and pupal development. Studying brain connectivity in the immature system opens up a potentially useful avenue of investigations since neurons have simpler morphologies and are greatly reduced in branching complexity.

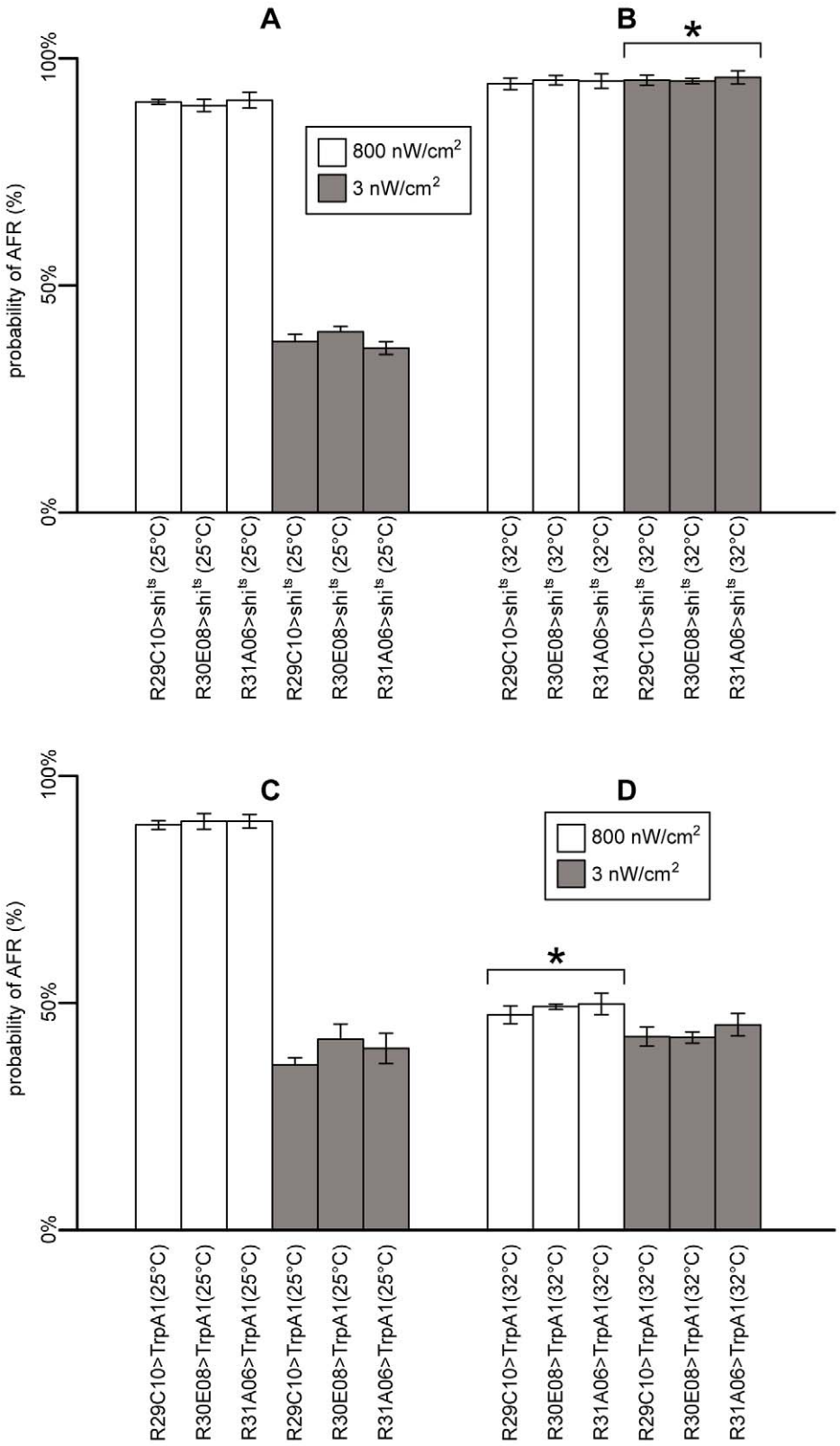

Figure 11. AFR rates in flies with silenced/overactivated DPLp2 interneurons. AFR rates in flies in which the DPLp2 interneurons were (A,B) silenced using a temperature-sensitive shibire mutant or (C,D) overactivated using dTrpA1. Flies were tested at 25°C (A,C; permissive for shibire) and 32°C (B,D; non-permissive for shibire) under both light (800 nW/cm^2) and dark conditions (3 nW/cm^2). At the lower temperatures, flies in both experimental conditions showed similar AFR rates to both controls (see Figure S3) and wild-type (see Figure 10). For each condition, five flies were measured for 100 trials and AFR rates were scored as described in Materials and Methods. Error bars indicate standard error of the means. Asterisks indicate (B) a significant increase of AFR rates in flies under dark conditions when DPLp2 interneurons were silenced with shibire at a non-permissive

temperature, and (D) a significant decrease of AFR rates in flies under bright light conditions when the DPLp2 interneurons were overactivated using TrpA1. Significance was determined as a $p<0.05$ using the chi-square test. See Figure S3 for AFR rates of constructs used.
doi:10.1371/journal.pbio.1000583.g011

We measured several network properties and found that the integration ability, clustering, functional segregation, small-worldness, and resiliency of the fly connectivity network were strikingly similar to those described of larger and more complex brain networks. Given the disparity in size and number of neurons between the mammalian nervous systems and that of the fly, we speculate that the similarity may reflect some shared functional constraints in complex nervous systems.

Materials and Methods

Fly Stocks

As wild-type stock we used Oregon R. Flies were grown under standard conditions at room temperature (25°C). MARCM clones were generated using flies of the genotype $GAL4_{C155}$, hsFLP; FRT42B, tubP-GAL80/FRT42B, UAS-mCD8::GFP.

We screened a database of adult brain expression patterns of 4,147 Gal4 lines (Rubin et al., unpublished) that had been constructed as described [18] and found the following five lines on the basis of the connectivity of the expressing neurons. Ocellar interneurons were targeted using the R29H12 line. Pre- and post-synaptic enrichment was studied using the R18H04 and R29C10 lines. Acute and ectopic neural inhibition/excitation was performed using the R18H04, R30E08, and R31A06 driver lines. See Figure S2 for the CNS expression pattern of these five lines.

Neuropile and cortex glia were visualized using Nrv2-Gal4 (BDSC stock # 6796) [63] to drive expression of UAS-cd8::GFP. Pre- and post-synaptic sites were visualized using the tau::LacZ (Bloomington stock number 5148) [64] and DSCAM::GFP [65] lines, respectively. Compound eye input was genetically disrupted using the eya^2 (BDSC stock # 2285). Genetically targeted neurons were inhibited and overactivated using w; UAS-$Shibire^{ts1}$ (BDSC stock # 1351) and w; UAS-dTrpA1/CyO [60], respectively.

Generation of MARCM Clones

For MARCM experiments [66], embryos of the appropriate genotype were collected on standard cornmeal/yeast/agar medium supplemented with live yeast over a 4 h time window and raised at 25°C for 21 to 25 h before heat-shock treatment. Heat-shock induction of FLP was done at 37°C for 60 min. The CNS was dissected in the late third instar.

Immunochemistry

Standard procedures were followed for antibody labeling [67]. Nervous systems were dissected from larvae and fixed in 3.7% buffered formaldehyde for 30 min at room temperature and then washed three times in PBT [phosphate buffered saline (pH 7.8) with 1% Triton-X100]. Fixed samples were blocked in 2% normal donkey serum (Jackson ImmunoResearch Laboratories, West Grove, PA, USA) in PBT for 30 min and then incubated in primary antibodies for 1 d at 4°C. Secondary axon tracts were visualized by labeling with Neuroglian (Nrg; Developmental Studies Hybridoma Bank BP104) and Fasciclin2 (Fas2; DSHB 2A12) antibodies diluted at 1:10. After washing off primary antibodies, tissues were incubated overnight at 4°C in secondary antibodies. Secondary antibodies were Cy3 conjugated anti-rat Ig (Jackson Laboratories) and FITC-conjugated anti-mouse Ig (Jackson Laboratories) used at a 1:100 dilution. After washing off secondary antibodies, tissues were mounted on poly-lysine coated coverslips, dehydrated, cleared through xylene, and mounted in DPX (Fluka, Bachs, Switzerland).

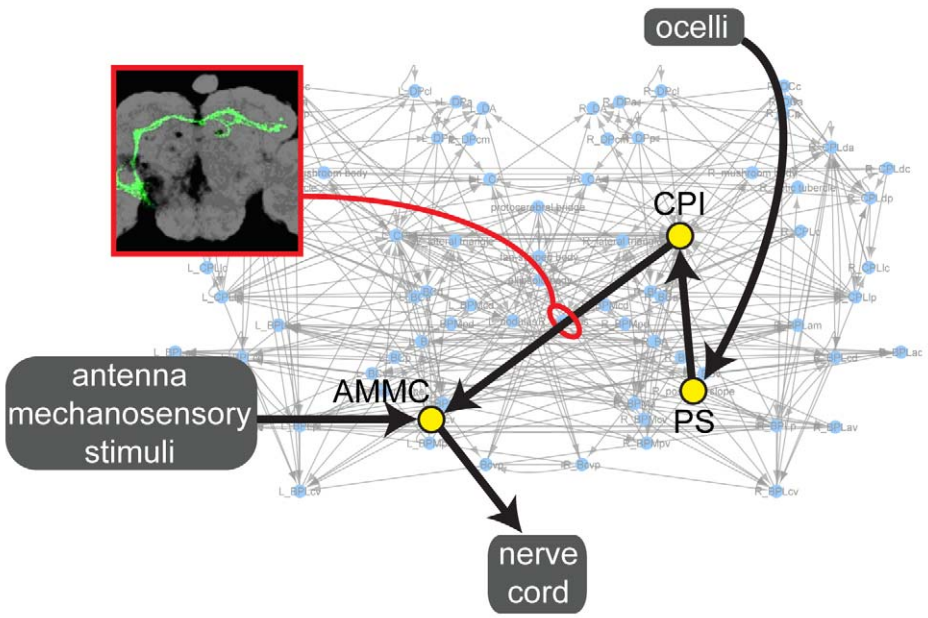

Figure 12. Whole-brain connectivity network for contextual interpretation of perturbations. In the center, the connectivity network schematic showing the network context of the experimentally addressed CPI to AMMC connection. The map indicates a putative circuit between the ocelli and the AMMC (leading to the nerve cord), which is mediated by the DPLp2 interneurons (shown in the top-left panel).
doi:10.1371/journal.pbio.1000583.g012

Electron Microscopy

Larval brains were dissected and fixed in 2% glutaraldehyde in PBS for 20 min, followed by a post-fixation for 30 min in a mixture of 1% osmium tetroxide and 2% glutaraldehyde in 0.15 M cacodylate buffer (on ice). Specimens were washed several times in PBS and dehydrated in graded ethanol and acetone (all steps on ice). Preparations were left overnight in a 1:1 mixture of Epon and acetone and then for 5–10 h in unpolymerized Epon. They were transferred to molds, oriented, and placed at 60°C for 24 h to permit polymerization of the Epon. Blocks were sectioned (0.1 μm). Sections were mounted on net grids (Ted Pella) and treated with uranyl acetate and lead citrate.

Measurement of Surface Area Coverage

Confocal stacks in which cortex and neuropile glia are labeled (Nrv2-Gal4>UAS-GFP) were manually segmented into the defined compartments [12]. For the boundary of each neuropile compartment, we used the visible morphology to classify each voxel into one of the following categories: (1) trachea, (2) neurite bundle, (3) glial sheath, and (4) adjacent neuropile. We defined the physical encapsulation ratio in Table 1 as the number of voxels in categories 1, 2, and 3 divided by the total number of boundary voxels.

Behavioral Assay

A fly is affixed ventral-side up to a coverslip using double-sided sticky tape. A probe is then used to mechanically deflect the arista, a feather-like appendage arising from the third antennal segment. We controlled for both light (provided by a Luxeon Star 4 LED and measured with a Mastech Professional Luxmeter, LX1010B photometer) and temperature (provided by a heating element controlled by a thermocouple placed near the fly). We digitized images of the fly at 30 Hz from above using a digital video camera attached to the eyepiece of a Zeiss dissecting microscope. Analysis of the imagery revealed that wild-type flies respond by extending either foreleg, which we term the antenna-foreleg response (AFR), with a mean time of response of 282 ms (SD = 119 ms). Trials were conducted by scoring for an AFR within 400 ms of antennal deflection (within 3 standard deviations), with a minimum inter-trial rest period of 4.6 s (typically 5 s). No habituation was observed. The experimenter was blinded to the genotype of animal being tested.

AFR rates were scored to assay both the influence of the ocelli versus the compound eye under light and dark conditions. In some experiments, black pigment (Schmincke Aerocolor 2887) was applied to either the compound eyes or ocelli to block light. Ocellar interneurons were targeted using the R29H12 line and the CPI-contralateral AMMC interneurons using the R29C10, R30E08, and R31A06 lines. Flies of all genotypes were tested for general locomotor behavior, UV light preference, and viability. All flies, with the exception of the visual performance of the compound eye blinded individuals, performed at levels similar to wild-type (unpublished data).

Complex Network Analysis

Connectivity networks were analyzed using the *Brain Connectivity Toolbox* [44] written in Matlab. *Cytoscape* was used to generate visualizations of the network [68].

Identifying Compartments of Sensory Integration Events

Given the characterization of compartments (in the connectivity network) innervated by several modalities (as described earlier), we computed, for each compartment, the number of connections each modality has to travel through to arrive at that compartment. This resulted in an eight-dimensional feature vector for every compartment (corresponding to the eight sensory modalities we characterized). For studying the sensory integration event of a selected pair of sensory modalities, we can then compute the aggregate number of connections required for sensory integration event at a given compartment by adding the number of connections traversed from each entry point of the respective sensory modality. Sorting the compartments using this aggregate number of connections results in a rank-ordered list of compartments, where the compartments with the lowest aggregate number are identified as the top candidates for studying sensory integration (see Table 4).

Network Reliability/Limitations

Each of the approaches taken suffers from its intrinsic biases, which we attempted to overcome by intelligently combining the resulting connectivity maps. We made use of various metrics during the construction phase of each map, which included looking for features that were inconsistent with what we know and expect; these included looking for disconnected nodes, nodes with no inputs, and nodes with no outputs. We then focused our attention on the affected nodes to determine and correct the source of error. The final consensus diagram contains two nodes that have no output (DA and DPcm) and three nodes that have no input (CPLc, DCp, and PS). In addition to technical limitations, these incongruities are likely to represent connections to entities outside of the described network (such as incoming sensory fibers, outgoing motor fibers, as well as inputs and outputs to the subesophageal ganglion and through the cervical connective to the ventral cord).

There are three important caveats that apply to the use and interpretation of the resulting network. First, the developmental approach only describes the secondary neurons that will form the adult brain (this includes 90%–95% of the population but misses the remaining primary neurons). We believe it is unlikely that the tract-based approach taken would describe these elements. Second, the described networks do not describe connectivity affected through neuromodulation. Behaviors that depend on such a connection, although not completely described even at this level, can only be provided with fragmentary information about their respective neural circuitry. Third, although the neuropile compartment schemes that exist are largely similar, incongruities exist between the schemes and so care must be taken in interpreting our results in the context of other schemes.

Supporting Information

Figure S1 MARCM clones in the larval brain. Central brains from wandering third-instar larva in which MARCM clones were induced. Shown are 27 preparations in which the 102 lineages of the central brain have been annotated among the stochastically induced set. Not shown are the four mushroom body lineages. The numbers indicate the lineages in which the filopodial tufts and bundle defasciculations have been measured (see Table S5 for lineage identification and compartmental position of each bundle protrusion).
Found at: doi:10.1371/journal.pbio.1000583.s001 (7.08 MB TIF)

Figure S2 Expression pattern of neuronal driver lines used. Maximum intensity projections of the entire CNS of the following five Gal4 lines: (A) R18H04, (B) R29C10, (C) R29H12, (D) R30E08, (E) R31A06. White arrows in (B), (D), and (E) indicate soma of the interneurons of the DPLp2 lineage.

Arrowheads in (C) indicate soma of the ocellar interneurons. Scale bar: 100 μm.
Found at: doi:10.1371/journal.pbio.1000583.s002 (4.31 MB TIF)

Figure S3 Control AFR rates. AFR rates of constructs used at both 25°C and 32°C under both (A) light (800 nW/cm^2) and (B) dark (3 nW/cm^2) conditions. AFR rates were indistinguishable from wild-type levels (see Figure 10A).
Found at: doi:10.1371/journal.pbio.1000583.s003 (0.18 MB TIF)

Table S1 Neuropile compartment abbreviation list. The nomenclature for neuropile compartments is defined elsewhere [12].
Found at: doi:10.1371/journal.pbio.1000583.s004 (0.05 MB DOC)

Table S2 Neurite bundle abbreviation list. The nomenclature for the neurite bundles is defined elsewhere [12].
Found at: doi:10.1371/journal.pbio.1000583.s005 (0.04 MB DOC)

Table S3 Tracts connecting compartments. List of tracts labeled with Neuroglian in the adult *Drosophila* central brain, organized by tracts which connect compartments ipsilaterally, contralaterally (via a commissure), or those related to the central complex (including the ellipsoid body, fan-shaped body, protocerebral bridge, lateral triangle, BCd/ventral body, and nodulus). The nomenclature (first column) and abbreviations (second column) have been defined in *Drosophila* [12,52,69] and are consistent with those assigned to *Musca domestica* [34]. Columns "Compartment A" and "Compartment B" refer to the compartments located at the tract endpoints. "Reference" column refers to published reports corroborating the tract as arborizing in the indicated pair of compartments. The "Distance" column provides a spatial indication of the distance between neuropile compartments being contacted by the tract. "Adjacent" indicates that the neuropile compartments are physically in contact with each other. "Short" indicates that the compartments at the tract endpoints are separated by, at most, one other neuropile compartment. "Long" indicates that there are two or more compartments in between the indicated pair.
Found at: doi:10.1371/journal.pbio.1000583.s006 (0.14 MB DOC)

Table S4 Tract-based connectivity matrix. This table is a connectivity matrix for tract-based interconnections between neuropile compartments in the *Drosophila* brain. Because these are based on the observation of structural bundles, each connection is undirected. The connections on either side are symmetrical, so only one side is shown. Each row shows whether the neuropile compartment on the first column has an observed structural tract with an endpoint to the compartments listed along the top. Columns show whether the compartments on the top have an observed tract to the areas listed along the left. Plus symbols (+) indicate the pathway is observed, see Table S3 for the tract name.
Found at: doi:10.1371/journal.pbio.1000583.s007 (0.36 MB DOC)

Table S5 Neuropile compartments contacted by each lineage. List of adult neuropile compartments in which filopodial tufts or defasciculations are observed along the neurite bundle of each lineage. The position of the bundle protrusions were derived from larval clones (see Figure S1) and the lineage immunochemistry using the Neurotactin antibody. The protrusions are divided into those occurring interstitially along the bundle, and those located at the bundle termination point. The abbreviations of lineages (first column) have been defined previously [22]. Branches of fasciculated bundles from single lineages are entered as separate branches, labeled h1, h2, and h3. The compartment nomenclature used [12] was selected because it is the only anatomical framework that has been characterized from the late larva to adult stages. The "ID" column refers to the clone number in Figure S1 that was used to derive the positions of the bundle irregularity. Clones for the four Kenyon cell lineages that form the mushroom body are not shown.
Found at: doi:10.1371/journal.pbio.1000583.s008 (0.15 MB DOC)

Table S6 Developmental lineage of neurons connecting compartments. List of putative connections between neuropile compartments derived by analysis of the lineages in the wandering third-instar larval brain. Lineages were determined to be potentially connected if their putative arborizations (from Table S5) occurred in the same neuropile compartment. In accordance with the directionality assumption of the model, we only permit connections in which the first interstitial branching position of a lineage occupies the same neuropile compartment as the terminal branching positions of another lineage. The "Distance" column indicates whether the putative connection is between adjacent compartments ("short") or not ("long").
Found at: doi:10.1371/journal.pbio.1000583.s009 (0.22 MB DOC)

Table S7 Matrix of developmental model of adult connectivity. This table is a connectivity matrix for the developmentally derived model of connectivity between neuropile compartments in the *Drosophila* brain. The connections on either side are symmetrical, so only one side is shown. Note that the model incorporates a hypothesis for directionality, so all connections are directed. Specifically, each column shows whether the neuropile compartment on the first row (top) has a developmentally predicted connection to each of the neuropile compartments listed on the first column (left). Plus symbols (+) indicate the pathway is predicted from developmental information; see Table S6 for the putatively connected lineages.
Found at: doi:10.1371/journal.pbio.1000583.s010 (0.36 MB DOC)

Table S8 Matrix of the consensus model of adult connectivity. This table is a connectivity matrix for the consensus model of connectivity between neuropile compartments in the *Drosophila* brain. The connections on either side are symmetrical, so only one side is shown. Note that the model incorporates a hypothesis for directionality, so all connections are directed. Specifically, each column shows whether the neuropile compartment on the first row (top) has a developmentally predicted connection to each of the neuropile compartments listed on the first column (left). Plus symbols (+) indicate the pathway is from tract-based or developmental evidence based on the described logic used to build a consensus.
Found at: doi:10.1371/journal.pbio.1000583.s011 (0.36 MB DOC)

Acknowledgments

We thank D. Chklovskii, V. Hartenstein, J. Simpson, and the referees for comments, criticisms, and suggestions of this work. We thank G. Rubin for allowing us to screen the imagery of Gal4 expression patterns and for providing the driver lines used in the behavioral assays prior to publication. We thank the Janelia Farm FlyLight project team for providing the imagery of the lines shown in Figure S2. We thank J. Simpson and T. Lee for providing the effector lines used for visualization and perturbation. We thank R.P. O'Connor for pointing out similar macrocircuitry work in the shark [21].

Author Contributions

The author(s) have made the following declarations about their contributions: Conceived and designed the experiments: WSP JWT. Performed the experiments: WSP. Analyzed the data: WSP PA EWM JWT. Contributed reagents/materials/analysis tools: WSP PA AJ. Wrote the paper: WSP PA JWT.

References

1. Brodmann K (1909) Localization in the cerebral cortex. Verlag von Johann Ambrosias Barth, Leipzig.
2. Devlin JT, Poldrack RA (2007) In praise of tedious anatomy. NeuroImage 37: 1033–1041.
3. Amunts K, Schleicher A, Zilles K (2007) Cytoarchitecture of the cerebral cortex—more than localization. NeuroImage 37: 1061–1065.
4. Paxinos G, Franklin KBJ (2004) The mouse brain in stereotaxic coordinates. San Diego: Academic Press.
5. Swanson LW (2004) Brain maps: structure of the rat brain. San Diego: Academic Press.
6. Gahr M (1990) Delineation of a brain nucleus: comparisons of cytochemical, hodological, and cytoarchitectural views of the song control nucleus HVc of the adult canary. J Comp Neurol 294(1): 30–36.
7. Ball GF, Absil P, Balthazart J (1995) Assessment of volumetric sex differences in the song control nuclei HVC and RA in zebra finches by immunocytochemistry for methionine enkephalin and vasoactive intestinal polypeptide. Brain Res 699(1): 83–96.
8. Brazis Paul W, Masdeu JC, Biller J (2001) Localization in clinical neurology (fourth edition). Philadelphia: Lippincott Williams & Wilkins.
9. Hartenstein V, Spindler S, Pereanu W, Fung S (2008) The development of the *Drosophila* brain. In Brain Development in *Drosophila melanogaster* GMTechnau, ed. New York: Springer New York. pp 1–31.
10. Jenett A, Schindelin JE, Heisenberg M (2006) The virtual insect brain protocol: creating and comparing standardized neuroanatomy. BMC Bioinformatics 7: 544.
11. Otsuna H, Ito K (2006) Systematic analysis of the visual projection neurons of *Drosophila melanogaster*. I. Lobula-specific pathways. J Comp Neurol 497(6): 928–958.
12. Pereanu W, Kumar A, Jenett A, Reichert H, Hartenstein V (2010) A development-based compartmentalization of the *Drosophila* central brain. J Comp Neur, doi:10.1002/cne.22376.
13. Pan Y, Zhou Y, Guo C, Gong H, Gong Z, et al. (2009) Differential roles of the fan-shaped body and the ellipsoid body in *Drosophila* visual pattern memory. Learn Mem 16: 289–295.
14. Strauss R, Hanesch U, Kinkelin M, Wolf R, Heisenberg M (1992) No-bridge of *Drosophila melanogaster*: portrait of a structural brain mutant of the central complex. J Neurogenet 8(3): 125–155.
15. Stocker RF (1994) The organization of the chemosensory system in *Drosophila melanogaster*: a review. Cell Tiss Res 275(1): 3–26.
16. Yorozu S, Wong A, Fischer BJ, Dankert H, Kernan MJ, et al. (2009) Distinct sensory representations of wind and near-field sound in the *Drosophila* brain. Nature 458(7235): 201–205.
17. Kamikouchi A, Inagaki HK, Effertz T, Hendrich O, Fiala A, et al. (2009) The neural basis of *Drosophila* gravity-sensing and hearing. Nature 458(7235): 165–171.
18. Pfeiffer BD, Jenett A, Hammonds AS, Ngo TB, Misra S, et al. (2008) Tools for neuroanatomy and neurogenetics in *Drosophila*. PNAS 105(28): 9715–9720.
19. Hartensten V, Cardona A, Pereanu W, Younossi-Hartenstein A (2008) Modeling the developing *Drosophila* brain: rationale, technique and application. BioScience 58(9): 823–836.
20. Herrick CJ (1943) The cranial nerves. A review of fifty years. Denison Univ Bull, J Sci Lab 38: 41–51.
21. Smeets WJAJ, Nieuwenhuys R, Roberts BL (1983) The central nervous system of cartilaginous fishes: structure and functional correlations. Berlin: Springer-Verlag.
22. Pereanu W, Hartenstein V (2006) Neural lineages of the *Drosophila* brain: a three-dimensional digital atlas of the pattern of lineage location and projection at the late larval stage. J Neurosci 26(20): 5534–5553.
23. Bohland JW, Wu C, Barbas H, Bokil H, Bota M, et al. (2009) A proposal for a coordinated effort for the determination of brainwide neuroanatomical connectivity in model organisms at a mesoscopic scale. PLoS Comput Biol 5(3): e1000334. doi:10.1371/journal.pcbi.1000334.
24. Felleman DJ, van Essen DC (1991) Distributed hierarchical processing in the primate cerebral cortex. Cerebral Cortex 1: 1–47.
25. Strausfeld NJ, Hansen L, Li Y, Gomez RS, Ito K (1998) Evolution, discovery, and interpretations of arthropod mushroom bodies. Learning & Memory 5: 11–37.
26. Homberg U (1989) Structure and functions of the central complex in insects. In: Gupta AP, ed. Arthropod brain: its development, structure and functions. New York: Wiley. pp 347–367.
27. Stocker RF, Lienhard MC, Borst A, Fischbach KF (1990) Neuronal architecture of the antennal lobe in *Drosophila melanogaster*. Cell Tiss Res 262: 9–34.
28. Pereanu W, Shy D, Hartenstein V (2005) Morphogenesis and proliferation of the larval brain glia in *Drosophila*. Dev Biol 283(1): 191–203.
29. Awasaki T, Lai SL, Ito K, Lee T (2008) Organization and postembryonic development of glial cells in the adult central brain of *Drosophila*. J Neurosci 28(51): 13742–13753.
30. Ito K, Awasaki T (2008) Clonal unit architecture of the adult fly brain. Adv Exp Med Biol 628: 137–158.
31. Larsen C, Shy D, Spindler SR, Fung S, Pereanu W, et al. (2009) Patterns of growth, axonal extension and axonal arborization of neuronal lineages in the developing *Drosophila* brain. *Dev Biol* 335(2): 289–304.
32. Zheng X, Zugates CT, Lu Z, Shi L, Bai J, et al. (2006) Baboob/dSmad2 TGF-b signaling is required during late larval stage for development of adult-specific neurons. EMBO 25: 615–627.
33. Rolls MM, Satoh D, Clyne PJ, Henner AL, Uemura T, et al. (2007) Polarity and intracellular compartmentalization of *Drosophila* neurons. Neural Dev 2: 7.
34. Strausfeld NJ (1976) Atlas of an insect brain. Berlin: Springer-Verlag.
35. Yokoi M, Mori K, Nakanishi S (1995) Refinement of odor molecule tuning by dendrodendritic synaptic inhibition in the olfactory bulb. PNAS USA 92: 3371–3375.
36. Bagri A, Cheng HJ, Yaron A, Pleasure SJ, Tessier-Lavigne M (2003) Stereotyped pruning of long hippocampal axon branches triggered by retraction inducers of the semaphoring family. Cell 113: 285–299.
37. Stanfield BB, O'Leary DDM, Fricks C (1982) Selective collateral elimination in early postnatal development restricts cortical distribution of rat pyramidal tract neurons. Nature 298: 371–373.
38. Truman JW, Schuppe H, Shepherd D, Williams DW (2004) Developmental architecture of adult-specific lineages in the ventral CNS of *Drosophila*. Development 131: 5167–5184.
39. Truman JW (1990) Metamorphosis of the central nervous system of *Drosophila*. Jour Neurobio 21(7): 1072–1084.
40. Williams DW, Truman JW (2004) Remodeling dendrites during insect metamorphosis. J Neurobiol 64(1): 24–33.
41. Varshney LR, Chen BL, Paniagua E, Hall DH, Chklovskii DB (2009) Structural properties of the *Caenorhabditis elegans* neuronal network. arXiv:0907.2373v2 [q-bio.NC].
42. Scannell JW, Blakemore C, Young MP (1995) Analysis of connectivity in the cat cerebral cortex. The Journal of Neuroscience 15(2): 1463–1483.
43. Young MP (1993) The organization of neural systems in the primate cerebral cortex. Proc Biol Sci 252: 13–18.
44. Rubinov M, Sporns O (2009) Complex network measures of brain connectivity: uses and interpretations. Neuroimage, doi:10.1016/j.neuroimage.2009.10.003.
45. Watts DJ, Strogatz SH (1998) Collective dynamics of "small-world" networks. Nature 393: 440–442.
46. Leicht EA, Newman MEJ (2008) Community structure in directed networks. Phys Rev Lett 100(11): 1187034.
47. Sporns O, Zwi JD (2004) The small world of the cerebral cortex. Neuroinformatics 2: 145–162.
48. Bassett DS, Bullmore E (2006) Small-world brain networks. Neuroscientist 12: 512–523.
49. Newman MEJ (2002) Assortative mixing in networks. Phys Rev Lett 89: 2087011–2087014.
50. Kintali S (2008) Betweenness centrality: algorithms and lower bounds. arXiv:0809.1906v0802.
51. Singh RN (1997) Neurobiology of the gustatory systems of *Drosophila* and some terrestrial insects. Microsc Res Tech 39(6): 547–563.
52. Strausfeld NJ, Vilinsky I, Hansen L (2000) FlyBrain: reduced silver sections. [http://flybrain.neurobio.arizona.edu/Flybrain/html/atlas/silver/index.html] doi: AA00037.
53. von Philipsborn A, Labhart T (1990) A behavioural study of polarization vision in the fly, *Musca domestica*. Jour Comp Physiol A167(6): 737–743.
54. Strausfeld NJ, Sinakevitch I, Okamura J (2007) Organization of local interneurons in optic glomeruli of the dipterous visual system and comparisons with the antennal lobes. Dev Neurobiol 67(10): 1267–1288.
55. Power ME (1946) The antennal centers and their connections within the brain of *Drosophila melanogaster*. J Comp Neurol 85(3): 485–517.
56. Liu L, Li Y, Wang R, Yin C, Dong Q, et al. (2007) *Drosophila* hygrosensation requires the TRP channels water witch and nanchung. Nature 450(7167): 294–298.
57. Frey BJ, Dueck D (2007) Clustering by passing messages between data points. Science 315(5814): 972–976.
58. Taylor CP (1981) Contribution of compound eyes and ocelli to sterring of locusts in flight. J Exp Biol 93: 1–18.
59. Kitamoto T (2001) Conditional modification of behavior in *Drosophila* by targeted expression of a temperature-sensitive shibire allele in defined neurons. J Neurobiol 47: 81–92.
60. Hamada FN, Rosenzweig M, Kang K, Pulver SR, Ghezzi A, et al. (2008) An internal thermal sensory controlling temperature preference in *Drosophila*. Nature 454(7201): 217–220.
61. Schmolesky MT, Wang Y, Hanes DP, Thompson KG, Leutgeb S, et al. (1998) Signal timing across the macaque visual system. J Neurophysiol 79: 3272–3278.

62. Tootell RBH, Reppas JB, Dale AM, Look RB, Sereno MI, et al. (1995) Visual motion aftereffect in human cortical area MT revealed by functional magnetic resonance imaging. Nature 375: 139–141.
63. Sun B, Xu P, Salvaterra PM (1999) Dynamic visualization of nervous system in live *Drosophila*. PNAS U S A 96(18): 10438–10443.
64. Callahan CA, Thomas JB (1994) Tau-beta-galactosidase, an axon-targeted fusion protein. PNAS 91(13): 5972–5976.
65. Wang J, Ma X, Yang JS, Zheng X, Zugates CT, et al. (2004) Transmembrane/juxtamembrane domain-dependent Dscam distribution and function during mushroom body neuronal morphogenesis. Neuron 43: 663–672.
66. Lee T, Luo L (2001) Mosaic analysis with a repressible cell marker (MARCM) for *Drosophila* neural development. Trends Neurosci 24(5): 251–254.
67. Ashburner M (1989) *Drosophila*. A laboratory manual. New York: Cold Spring Harbor Laboratory Press. pp 214–217.
68. Shannon P, Markiel A, Ozier O, Baliga NS, Wang JT, et al. (2003) Cytoscape: a software environment for integrated models of biomolecular interaction networks. Genome Res 13(11): 2498–2504.
69. Ito K (1994) Ito's brain sections. [http://flybase.org/data/images/Contributed-Images/brain-k-ito/].
70. Neuser K, Triphan T, Mronz M, Poeck B, Strauss R (2008) Analysis of a spatial orientation memory in *Drosophila*. Nature 453(7199): 1244–1247.
71. Wang Z, Pan Y, Li W, Jiang H, Chatzimanolis L, et al. (2008) Visual pattern memory requires foraging function in the central complex of *Drosophila*. Learn Mem 15(3): 133–142.
72. Ilius M, Wolf R, Heisenberg M (2007) The central complex of *Drosophila melanogaster* is involved in flight control: studies on mutants and mosaics of the gene ellipsoid body open. J Neurogenet 21(4): 321–338.
73. Baker DA, Beckingham KM, Armstrong JD (2007) Functional dissection of the neural substrates for gravitaxic maze behavior in *Drosophila melanogaster*. J Comp Neurol 501: 756–764.
74. Liu G, Seiler H, Wen A, Zars T, Wolf R, et al. (2006) Distinct memory traces for two visual features in the *Drosophila* brain. Nature 438(7076): 551–556.
75. Krashes MJ, DasGupta S, Vreede A, White B, Armstrong JD, et al. (2009) A neural circuit mechanism integrating motivational state with memory expression in *Drosophila*. Cell 139(2): 416–427.
76. Bausenwein B, Muller NR, Heisenberg M (1994) Behavior-dependent activity labeling in the central complex of *Drosophila* during controlled visual stimulation. J Comp Neurol 341(2): 255–268.
77. Mappes M, Homberg U (2007) Surgical lesion of the anterior optic tract abolishes polarotaxis in tethered flying locusts, Schistocerca gregaria. J Comp Physiol A 193(1): 43–50.
78. Greenspan RJ, Finn JA, Hall JC (1980) Acetylcholinesterase mutants in *Drosophila* and their effects on the structure and function of the central nervous system. J Comp Neurol 189(4): 741–774.